WAVE MODIFICATIONS IN A SEMI–ENCLOSED BASIN: BAHIA CONCEPCION

By

HANDE CALISKAN

A THESIS PRESENTED TO THE GRADUATE SCHOOL
OF THE UNIVERSITY OF FLORIDA IN PARTIAL FULFILLMENT
OF THE REQUIREMENTS FOR THE DEGREE OF
MASTER OF SCIENCE

UNIVERSITY OF FLORIDA

2006

Copyright 2006

by

Hande Caliskan

ACKNOWLEDGMENTS

I would like to thank to my advisor Arnoldo Valle–Levinson for his substantial help, moral support and patience throughout this study, my committee members Robert G. Dean and Andrew B. Kennedy for assisting me with their valuable knowledge, and Alexandru Sheremet for helping me to find the suitable model for my study.

I also would like to thank to my wonderful parents, for their endless love and trust in me and finally my friends for their incredible support.

Nothing would be as good as it is right now without you…

TABLE OF CONTENTS

LIST OF TABLES

LIST OF FIGURES

Abstract of Thesis Presented to the Graduate School
of the University of Florida in Partial Fulfillment of the
Requirements for the Degree of Master of Science

WAVE MODIFICATIONS IN A SEMI-ENCLOSED BASIN: BAHIA CONCEPCION

By

Hande Caliskan

December 2006

Chair: Arnoldo Valle-Levinson
Major: Coastal and Oceanographic Engineering

In order to determine wave climatology in Bahia Concepcion, yearlong records of bottom pressure were obtained at the mouth and head of the bay. Wind waves were predominantly produced by southeastward winds in the winter and north–northwestward winds in the summer. Only 3, 7 and 15 second waves were recorded at the mouth of the bay, i.e. wave energy was produced only by 3, 7 and 15 second waves there. At the head of the bay 3 second waves dominated the wave energy. The energetic long-period swell waves were dissipated in the bay as they were not observed at the head of the bay. This study sought to identify the effects that caused the swell waves to attenuate in the bay. Numerical model results showed that long-period swell waves were attenuated because of the combined effects of bottom friction, refraction, diffraction and wave blocking. Most of the attenuation, however, was caused by wave blocking owing to the change of orientation of the bay.

CHAPTER 1
INTRODUCTION

Wave Climatology in semi-enclosed basins has been studied numerous times at different sites all around the world. One of the common findings in these studies has been the observation that ocean swell vanishes at some distances into the bay. For example, Boon et al., (1996) observed that in Chesapeake Bay ocean swell waves were attenuated before they reach the middle of the bay. Similarly, according to Long and Oltman-Shay's (1991) observation ocean swell waves attenuated at the open coast of Duck, NC. According to their study in 1991, two dimensional wave spectra were used at two different points, one of which was closer to the coast. One of the observations was that wave frequency was higher and direction was nearly perpendicular to the bottom contours at the point closest to the coast. At the offshore point, frequency was lower and waves were propagating with a greater approach angle. This observation has been used to hypothesize that the cause of the attenuation of ocean swell waves was refraction. To my knowledge, this hypothesis has been the only attempt to explain the reason for the attenuation of swell waves.

This study is motivated by the observation that low frequency waves (~ 7 s) were dissipated in Bahia Concepcion, in the Gulf of California (Figure 2-1). In-situ data recorded at two different stations suggested the influence of waves with periods of 5 – 7 s at the entrance but waves with periods less than 5 s at the head. However, the main purpose of the data collection was determining along-bay pressure gradients. Data were recorded according to the requirements of the main purpose that might not have had appropriate temporal coverage to yield a reliable set of data for wave climatology studies. In order to test the concept of wave attenuation in Bahia Concepcion a numerical wave model, SWAN, was used first to be able to validate the reliability

of the data, secondly to find the possible reasons behind the attenuation and finally to show the contribution of various dissipating effects on attenuation.

The study area is located on the Gulf of California side of the Baja California peninsula between the longitudes of -111° 58' 8" and -111° 40' 6" and the latitudes of 26° 32' 21" and 26° 54' 57" (Figure 2-1). Bahia Concepcion is exposed to strong winds from NW with a speed more than 10 m/s for extended periods along its axis during the winter and spring seasons (Badan–Dangon et al., 1991). Its bathymetry is quite simple. Immediately after the bay entrance, there is a deep and narrow channel with an average depth of 30 m at the east side of the bay mouth. The deepest point of the bay is located on this channel and the depth there is 34.5 m. The bay entrance, with a width of 5.95 km, is located 39.98 km away from its south end point and the bay width varies between 3.40 and 10.38 km. The west side of the bay, close to the mouth, has the mildest bed slope causing an extended shallow zone from the coast. In this shallow zone, between the latitudes of 26° 42′ 31″ and 26 ° 45′ 13″ there are several islands. The names of the islands are Isla San Ramon, Isla Pitahaya, Isla Blanca, Isla Bargo, Isla Guapa and Tecomate.

Semi-diurnal tidal height is observed to be 150 cm at the entrance and 36 cm at the head of Gulf of California. The minimum semi-diurnal tidal height in the Gulf of California is observed in its central regions with a value of 5 cm because of the existence of an semi-diurnal amphidromic point. (Marinone et al., 2003). Since Concepcion bay is located at the Central Gulf of California, tidal forcing along the bay is weak.

CHAPTER 2
METHODS

In order to determine along–bay pressure gradient, bottom pressure was recorded every 15 min at the mouth and head of the bay (Figure 2-1). These measurements were obtained between November 2004 and October 2005. Data were recorded with SBE26 instruments deployed at a depth of 5.10 m at the mouth and 5.70 m at the head of the bay, below the mean sea level and these stations are labeled as ST1 and ST2, respectively (Figure 2-1). In the mean time, wave data were recorded with a frequency of 4 Hz at 30 s bursts every 3 hrs.

One of the most important inputs for determining the surface wave field is the wind data because of its high contribution to wave development and growth. For this study, wind data (wind velocity) were recorded using Aanderaa anemometers with a frequency of 1 Hz. For this purpose instruments were installed 10 m above the mean sea level at the mouth and the head, at distances less than 1 km from the bottom pressure recording stations, ST1 and ST2.

Although it was possible to measure wind waves with the available instruments, there was no *a–priori* intention of resolving the wave field. Once again, the main purpose of the deployment was to observe the pressure gradients along the bay. But in order to assess whether the wind wave patterns observed were reliable, Concepcion Bay was modeled using the Simulating Waves Nearshore Model (SWAN Model). The latest version available for public use, SWAN Cycle III version 40.41, was used for this study.

Wave prediction models have been improved according to the improvements on the wave evolution knowledge. First generation models did not consider nonlinear wave interactions while second generation models included these interactions through some parameterizations. On the other hand, third generation wave models used an explicit source term for non-linear wave interactions (Hasselmann et al., 1985). SWAN is a third generation, numerical wave prediction

model that uses the known bathymetry, wind and current conditions for wave parameter estimations. The model uses the wave action balance equation, which can be expressed in Cartesian coordinates as (Hasselmann et al., 1973)

$$\frac{\partial N}{\partial t}+\frac{\partial\left(c_x N\right)}{\partial x}+\frac{\partial\left(c_y N\right)}{\partial y}+\frac{\partial\left(c_{\omega'} N\right)}{\partial \omega'}+\frac{\partial\left(c_\theta N\right)}{\partial \theta}=S_T$$

where N (ω', θ) (= E(ω, θ)/ ω') is the action density, E(ω, θ) is the wave energy density, ω' is the intrinsic frequency (i.e., frequency of wave components according to a reference moving with the local current), t is time, S_T is the source term, θ is the wave direction and c_x, c_y, $c_{\omega'}$, c_θ are the propagation velocities in x, y, ω' and θ spaces, respectively. Each term of this equation can be explained as follows:

$\frac{\partial N}{\partial t}$ = Local rate of change of action density,

$\frac{\partial\left(c_x N\right)}{\partial x}$ = Propagation of action in x direction,

$\frac{\partial\left(c_y N\right)}{\partial y}$ = Propagation of action in y direction,

$\frac{\partial\left(c_{\omega'} N\right)}{\partial \omega'}$ = Shifting of relative frequency due to depth and current variations,

$\frac{\partial\left(c_\theta N\right)}{\partial \theta}$ = Refraction due to depth and current variations,

S_T = Source term for wave energy growth due to wind, wave energy transfer due to nonlinear wave–wave interactions and wave energy dissipation due to bottom friction, depth induced breaking and whitecapping.

For this study, inputs to the model were bathymetry, wind velocity and wave forcing. A southeastward wind of speed 10 m/s is used for the base case of the study because the bay is

exposed to southeastward winds with speeds exceeding 10 m/s for extended periods. In addition, waves were prescribed from the N boundary with an approach angle of 30^{o}, a wave height of 1.5 m and a wave period of 10 s. The reason for prescribing waves with these parameters is to represent the ocean swell waves entering the bay to be able to observe the changes that will occur as they propagate towards the head. The outputs requested from the model were one dimensional (frequency) spectra, significant wave height, mean wave direction, energy dissipation, average absolute wave period and mean absolute wave period. For all tests, nonlinear quadruplet wave interactions, depth induced wave breaking, whitecapping, bottom friction and wind generation were activated to be able to obtain closer results to real life conditions.

SWAN has three optional formulations for friction calculations, which are:

- The empirical JONSWAP model (Hasselmann et al., 1973),
- Eddy viscosity model of Madsen et al. (1988),
- Drag law model of Collins (1972).

Using the available data it is not possible to make a calibration for bottom friction. Therefore, in order to decide what friction formulation to use, a test was conducted. Three different cases were run with the same boundary conditions, same southward wind of speed 10m/s. The only parameter changed for these cases was the friction model. Although friction factors within each formulation can be modified as required, default values were used for this test. Figures 2-2 and 2-3 show contour plots of significant wave height and energy dissipation over the bay for the three friction models. According to the results obtained from this test, there was not much difference in the general patterns of the contour plots. However, it was clear that the model of Collins gave lower estimates of friction than both JONSWAP and Madsen's model. When the models of Collins and Madsen were compared, it was seen that the greatest difference in energy dissipation was 0.1843 W/m^2 at the mouth of the bay and was in the range of 0.18 – 0.49 W/m^2

along the breaker zone where most of the waves break. There is a ~20 m shoal at the mouth of the bay between the longitudes of -111° 52′ 56″ and -111 ° 52′ 12″ and latitudes of 26° 51′ 23″ and 26 ° 52′ 41″ (Figure 2-1). The depth decreases by 6 m at the bar and it is very likely that waves feel the bottom and dissipate on it. The model of Collins gave low estimates for energy dissipation over this bar and therefore JONSWAP and Madsen formulations were considered further.

When JONSWAP and Madsen's models were compared it was seen that Madsen's model gave greater energy dissipation values. The largest difference between the model estimates was at the mouth, on the shoal, with a value of 0.17 W/m^2. Even though the dissipation estimates were slightly different from each other, this only affected the significant wave height by 1.8cm. Since this difference was very small when compared to the wave height it can be said that Madsen's formulation produced consistent results with JONSWAP for this specific case. According to the test results and knowing the fact that SWAN uses JONSWAP model as its default setting, JONSWAP was chosen to be used in this study. Default values for the coefficient of the JONSWAP formulation are: 0.038 m^2/s^3 for swell conditions and 0.067 m^2/s^3 for wind sea conditions. In this study, both swell and local wind waves exist but SWAN does not have a default value to consider both swell and wind sea conditions and with the available data it was not possible to make a calibration for the JONSWAP formulation coefficient. Therefore, both coefficients for swell and wind sea conditions were tested and it was observed that when the coefficient for swell conditions was used dissipation values were too small to be realistic and therefore, 0.067 m^2/s^3 was used for the rest of the study.

Secondly, a sensitivity test for the model spatial resolution was conducted. The computational grid that was used to generate results was determined using this sensitivity test.

For this test, three different grid sizes were selected for the same wind speed and direction to observe the sensitivity of the calculations to the resolution. A southeastward wind with a speed of 10 m/s (the predominant wind direction for the bay in winter), was selected to drive the model with grid sizes of 100, 200 and 400 m both in the x and y axes. When compared to the finest grid (100m), the 400m grid size was unable to resolve the details properly especially along the shore due to inaccurate values obtained by interpolating a point inside the bay where the wave parameters can be calculated and a point outside the bay where wave parameters cannot be calculated. On the other hand, the grid size of 200m was able to resolve the bay better than 400m showing enough details for the purpose of this study.

Figure 2-4 shows a comparison of these three grids for significant wave height calculations. As the grid size increases, the model tends to overestimate the significant wave height. The percent difference of significant wave heights between the grid sizes of 100m and 200m was less than 1% whereas between 100m and 400m, the difference increased to 4% along the mid-span of the bay. Moreover, increasing the grid size made the model unable to resolve the details along the shoreline. For example, using a grid size of 400m caused the islands, between the longitudes of -111^{o} 54′ 8″ and -111 ^{o} 51′ 43″ and the latitudes of 26^{o} 42′ 31″ and 26 ^{o} 45′ 13″, to disappear. On the other hand, a grid size of 200m was not only able to show enough details for the purpose of the study, but also it saved a considerable amount of CPU and wall-clock time (Table 2-1). The grid size of 200 m was chosen for the rest of the studies because it achieved the required resolution and it saved a considerable amount of time for each run.

After determining the grid size, different cases for different wind speeds and directions were run. The main purpose of these tests was

- to compare the behavior of waves at ST1 and ST2, where observations were available;

- to compare different model results with the available observational data;
- to observe the behavior of waves under different wind speed conditions; and
- to observe the differences due to different wind directions under a constant wind velocity.

First of all, the sensitivity of the wave parameters, such as significant wave height, wave period and mean wave direction, to wind speed variability was tested with a fixed azimuth of 150^{o} and wind speeds of 5, 10 and 15 m/s. It should be noted that, here and throughout this study, wind and wave directions will be presented according to oceanographic convention. In other words, the direction where the wind is blowing (or the wave is propagating), is measured clockwise from the North. Secondly, wind speed was kept constant at 10 m/s and variability of the wave parameters as a result of the wind direction change was observed. All test cases are summarized in Table 2-2.

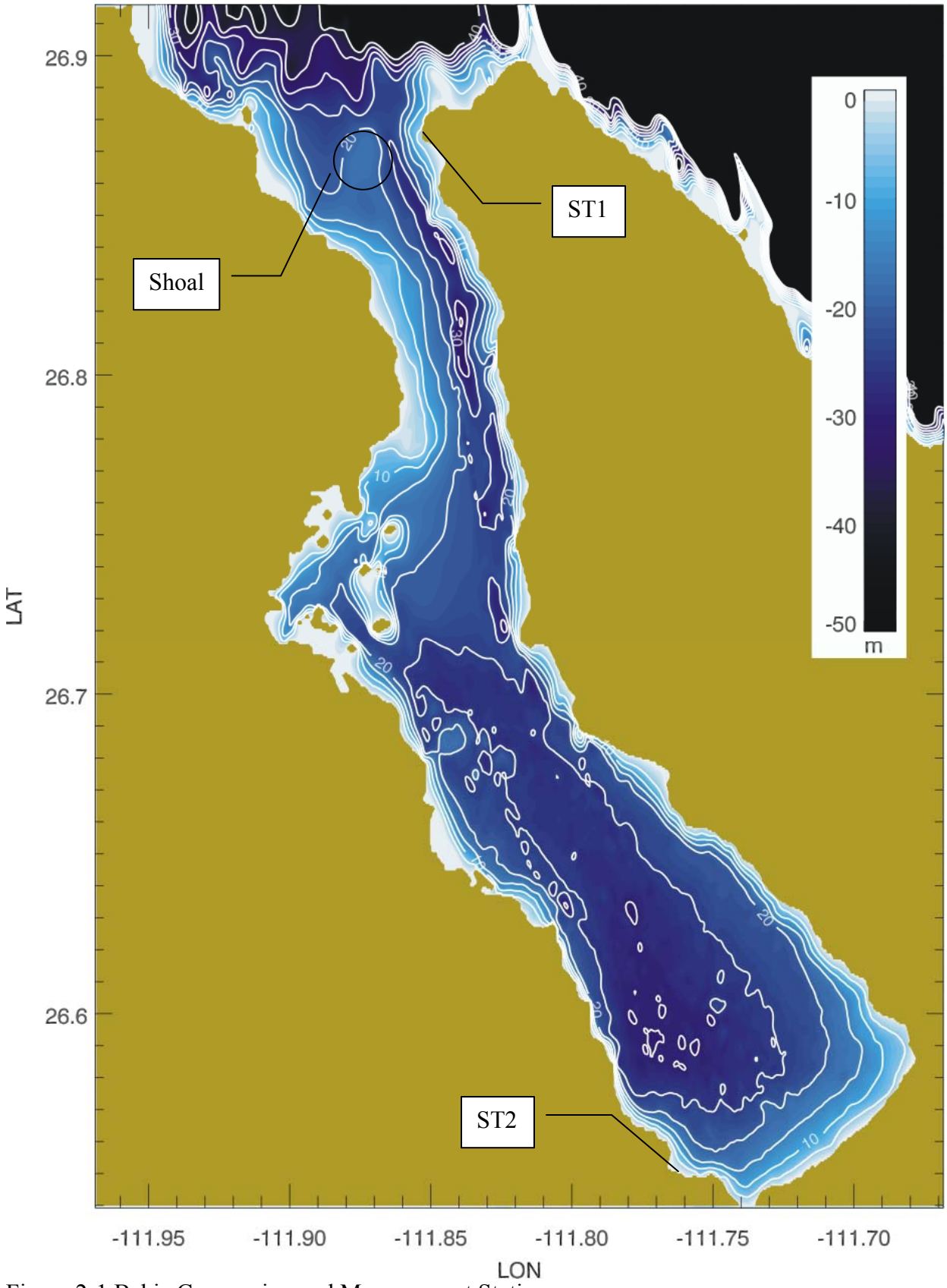

Figure 2-1 Bahia Concepcion and Measurement Stations

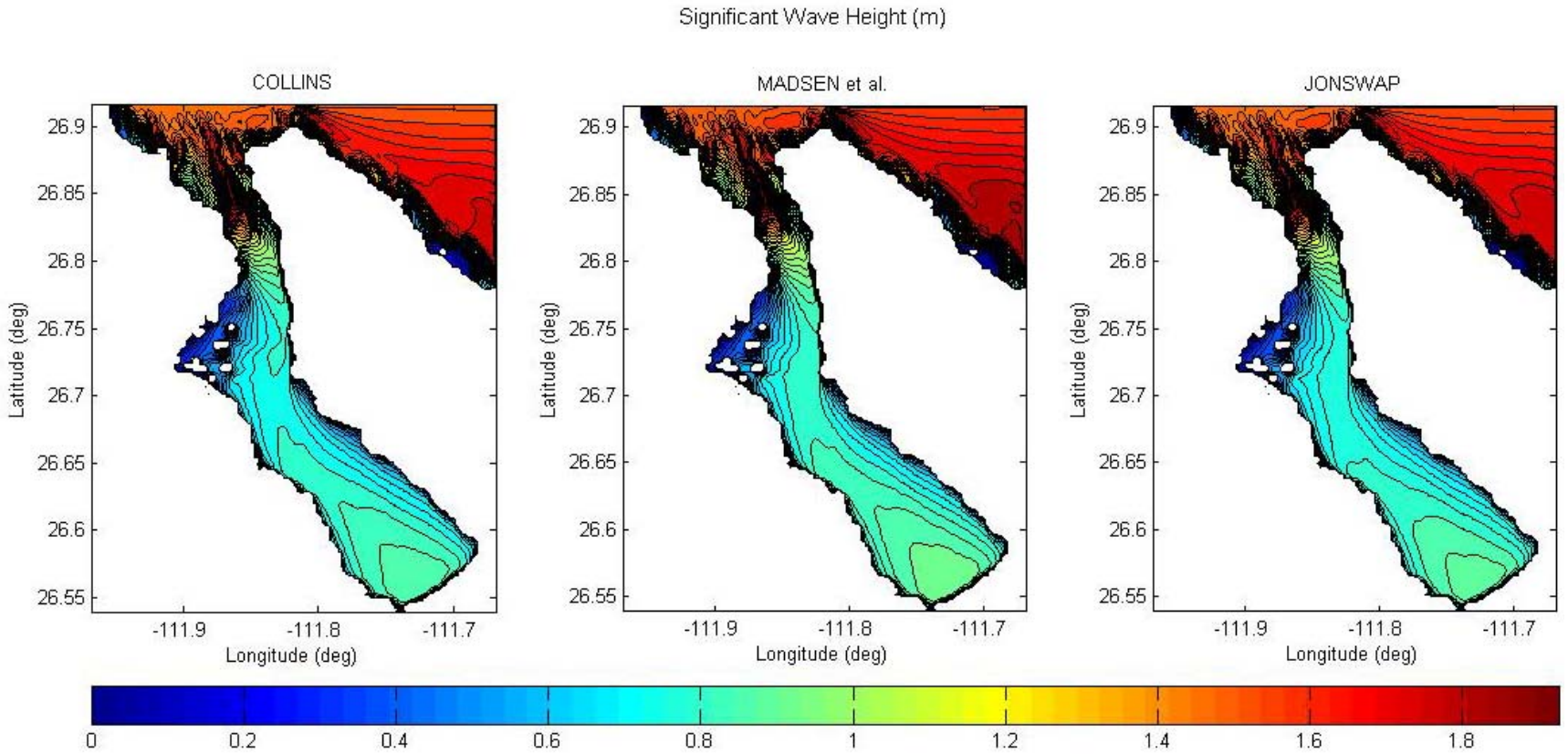

Figure 2-2 Comparison of Contour Plots of Significant Wave Height for Available Friction Models in SWAN Wave Model

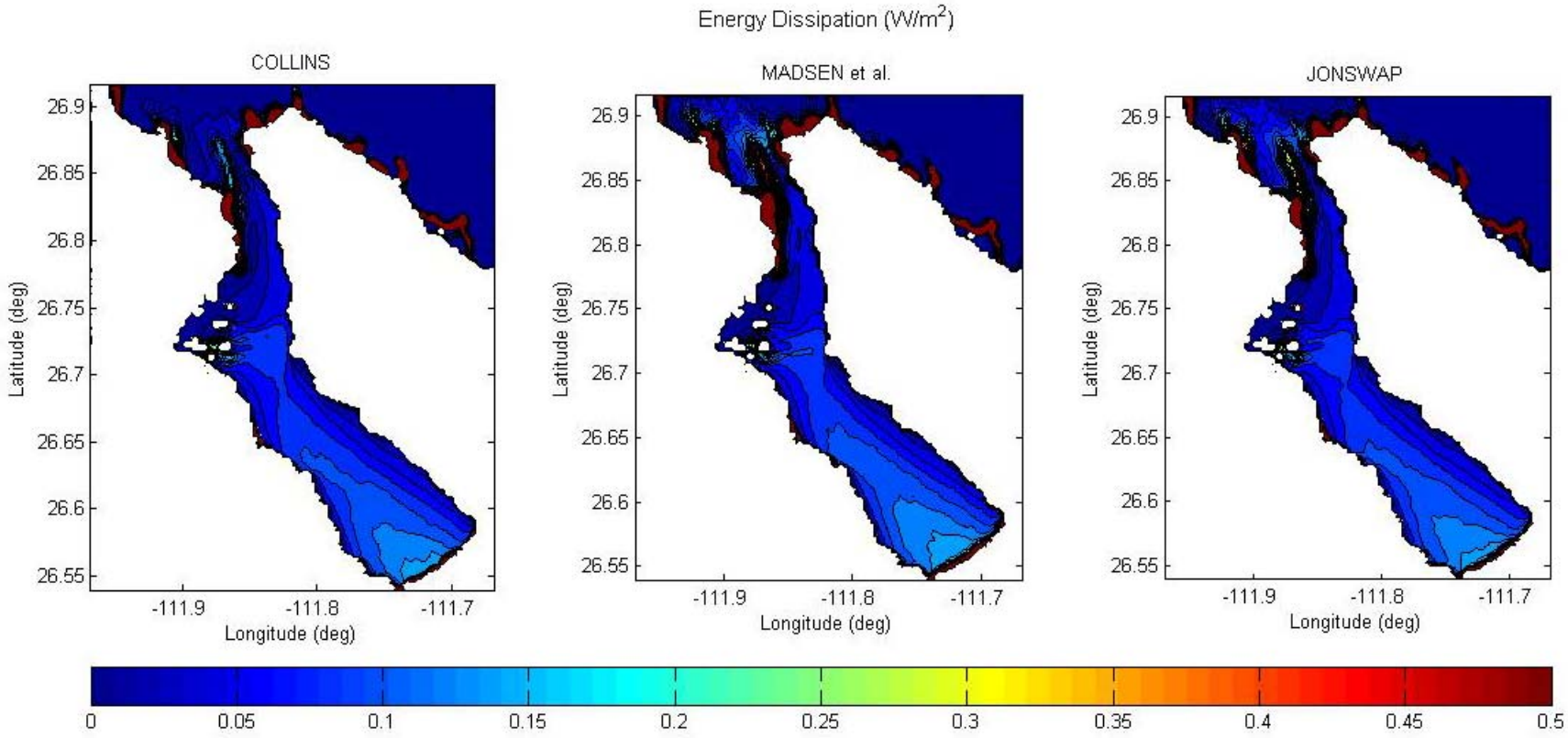

Figure 2-3 Comparison of Contour Plots of Energy Dissipation for Available Friction Models in SWAN Wave Model

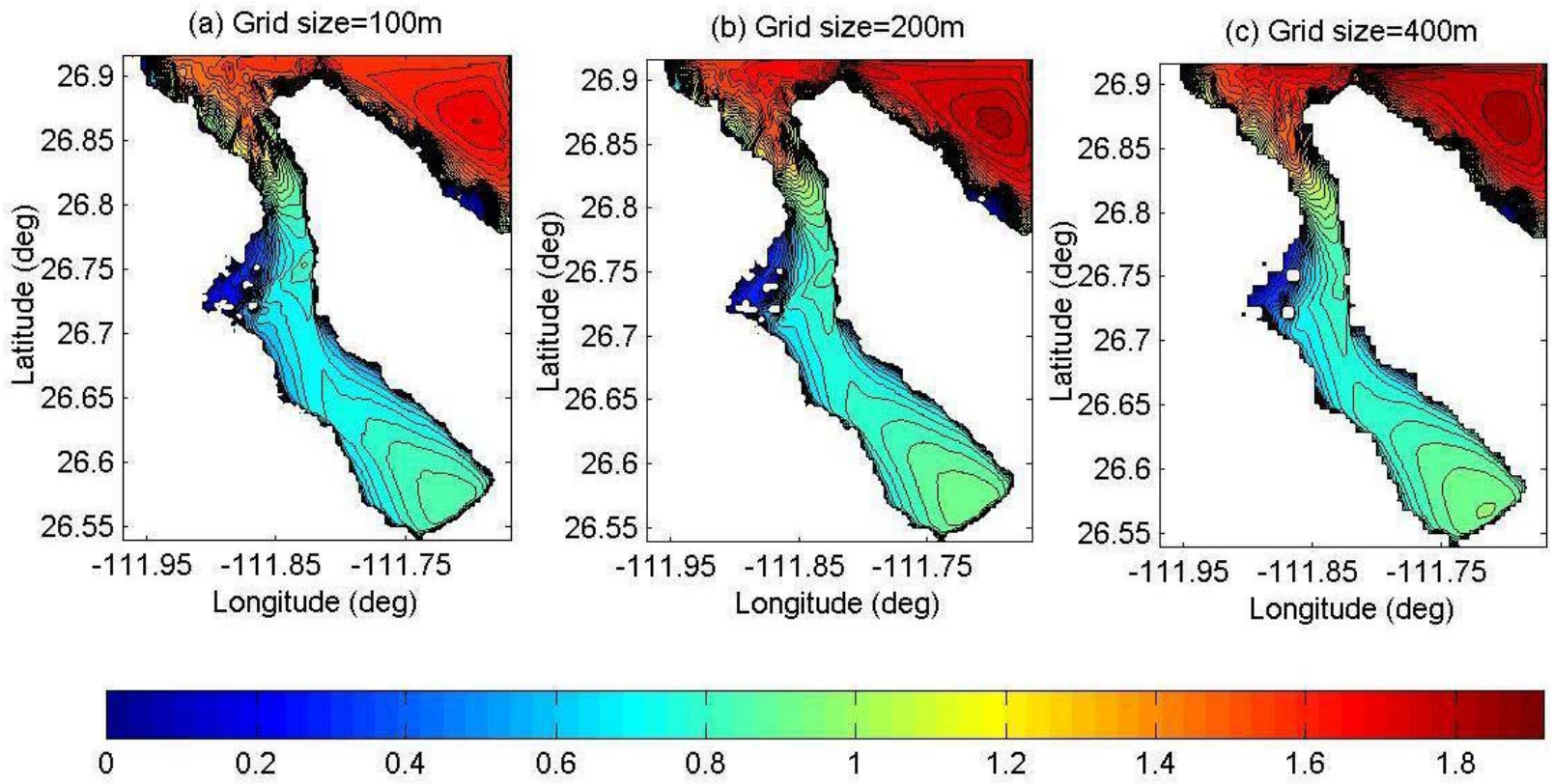

Figure 2-4 Contours of Significant Wave Height for Different Grid Sizes

Table 2-1 CPU and wall-Clock times for three different grid sizes

Grid Size (m)	100	200	400
Total CPU Time	7029.81	1725.39	394.98
Total Wall-Clock Time (s)	46240.12	1871.61	413.74

Table 2-2 Test cases

Name of the Case	Wind Speed (m/s)	Wind Direction (^{o})
BC1	5	150
BC2	10	150
BC3	15	150
BC4	10	180
BC5	10	120
BC6	10	50
BC7	10	20
BC8	10	90
BC9	10	0

CHAPTER 3
RESULTS AND DISCUSSION

This chapter contains two sections. In the first section of this chapter, results derived from the data collected by the bottom mounted instruments will be presented. The second section includes the detailed model results and a comparison of them with the observational results.

Observational Results

As mentioned before, wind velocity data were recorded at ST1 and ST2 with a frequency of 1 Hz. To be able to eliminate high frequencies in the wind data, Lanczos filter, which is a low–pass digital filter, was used. Then wind velocity vectors are decimated and plotted for every 3 hrs over the full deployment duration at the mouth (Figures 3-1b – 3-5b) and at the head (Figures 3-6b – 3-10b). In these plots, direction of the vectors demonstrates where the wind is blowing to and magnitude of the vectors demonstrates its speed. The scale for the speed is shown on the y-axis in m/s. It should also be noted that there were missing data due to recording problems, especially at the mouth of the bay. These periods are marked with a horizontal dashed line plotted at zero velocity to differentiate the recording durations.

Figures 3-1a – 3-10a show contours of wave energy, plotted in time and frequency space. As a matter of fact, in these plots, each section cut vertically would represent the wave spectrum of a burst that was recorded at the time of the selected section. The reason for plotting these wavelets was to give a better representation of the observed wave energy with different frequencies over the full deployment duration. Energy (in cm^2) here is defined to be the sum of the variances over each frequency band. For example, contours plotted for a wave period of 7 s show the sum of the variances for the frequencies between 1/8 and 1/6 Hz.

Figures 3-1a – 3-10a and 3-1b – 3-10b are presented for the same periods of time and plotted one on another to be able to show the high correlation between wind velocity and wave

action. As the data suggest, when wind speed increases, wave action usually increases too. However, for the cases of strong eastward or westward winds, it is not possible to observe this correlation. The main reason for this weak correlation is the short fetch in the east – west direction. The data suggest that wave action in the bay is highly correlated with the speed of winds blowing along the axis of the bay (winds from NW – NE) because of its longer fetch that allows waves to grow.

Contour plots at the mouth of the bay (Figures 3-1a – 3-5a) show that wave energy is mostly concentrated on 3–7 s waves and it is possible to observe some energy on 13–15 s waves. However, in reality more energy could be concentrated on low frequency waves (i.e. periods of 13–15 s or more). It is not possible to observe this with the available data because each burst consisted of a 30 s recording interval. Such an interval may not be enough to capture enough number of low frequency waves to be able to show the actual energy they have.

On the other hand, the data set for the head of the bay shows that wave energy has decreased considerably although wind speed has not decreased more than 20%. For instance, 13-15 s waves have completely disappeared, it is not possible to observe as much energy on 5–7 s waves as at the mouth and even the energy on 3 s waves that can be produced by local winds has decreased considerably. (Figures 3-1b – 3-5b)

The reduced wave activity at the head of the bay is either caused by transfer or by loss of wave energy and the reasons for that might be refraction, shoaling, bottom friction, whitecapping or any combination thereof. To see if the computational model will give similar results to what has been observed and to be able to understand the reasons of low frequency wave attenuation at the head, the SWAN wave model has been run and results obtained are presented in the following section.

SWAN Wave Model Results

Figures 3-12, 3-13 and 3-14 show the spectral energy density distributions in $J/m^2/Hz$ derived from the SPEC1D command of SWAN model, which gives the one–dimensional spectra, for all of the test cases presented in Table 2-2. These contours were plotted for the frequency range 0.05–0.5 Hz using the spectra that were obtained at 20 different points selected approximately in the middle of the bay from mouth to head. Coordinates of the selected points are presented in Table 3-1 and locations are shown in Figure 3-11 with a star. The ordinate axis of the contour plots show the distances from the head in meters meaning that the zero point shows the mouth of the bay.

All contours, regardless of wind speed and direction, show that the bay has a behavior of attenuating the highly energetic long waves as they propagate toward the head. It is possible to see that approximately around 15 km from the mouth most of the low frequency waves were dissipated in all cases. On the other hand, higher frequency waves exist everywhere along the bay. This behavior was also one suggested by the field data. Therefore, model results suggest that observational data presented in the previous section have a revealing pattern of the wave behavior in the bay.

As mentioned previously, BC1, BC2 and BC3 cases were run to see the response of the bay to wind speed change under the same wind direction and wave forcing conditions. Energy density contours of these cases are presented in Figure 3-12. One of the major differences in these three plots is the frequency range of waves at the head of the bay. It is seen that the frequency range at the head of the bay increases as the wind speed increases. For BC1, wind speed is 5 m/s and the frequency of most of the waves reaching the head ranges between 0.28 and 0.50 Hz, giving a range interval of 0.22 Hz. For BC2 where the wind speed is 10 m/s this range is between 0.18 and 0.50 Hz causing the interval to increase to 0.32 Hz. The frequency

range for BC3 (wind speed = 15 m/s) is between 0.14 and 0.50 Hz and the range interval is 0.36 Hz. This suggests that stronger winds can generate waves with a wider range of frequencies when compared to weaker winds.

The response of the bay to the wind direction change is displayed by the energy density contours for BC2 and the cases BC4 - BC7 (Figures 3-12, 3-13, 3-14). When the bay is under the effect of southward - southeastward winds, (Figures 3-12 and 3-13 for BC2, BC4 and BC5) energy contours were very similar to each other. In other words, even adverse winds did not affect the distance traveled by the swell waves. The only difference observed was at the locally generated short wind waves.

When the wind was blowing from between west and south; the distance, along which the low frequency waves attenuated, was equal to the distance for cases BC2, BC4 and BC5. However, the frequency of the waves that reached the head of the bay decreased considerably. This is due to the effect of the adverse wind and the direction the prescribed waves at the mouth of the bay. Since the wind was blowing from the opposite direction, waves were dissipated as they propagated towards the head. This caused the frequency of the waves that were able to reach to the head to further decrease. (Mitsuyasu, 1997)

As stated previously, attenuation of low frequency waves was observed from the *in-situ* data and the SWAN model was used to verify the reliability of the observational results. Since the model results verified that the observational results were reliable, the SWAN model results were also used to determine the reasons for attenuation of the low frequency waves as they propagated towards the head. As mentioned before, significant wave height, mean wave direction, average wave period and energy dissipation outputs were requested from the model.

These parameters are presented in contour maps and used both for reinforcing the observational results and finding a reasonable explanation to what has been observed (Figures 3-15 – 3-26).

Significant wave height (H_s) contour maps show that for all cases, H_s decreases considerably from the mouth to a distance of 6 km into the bay (Figures 3-15 – 3-17). This attenuation mainly occurs on the west side of the bay entrance. The 30 m deep channel on the east side of the mouth does not have a significant effect on H_s attenuation. Further into the bay, H_s increases slightly for the case of southward and southeastward winds (for cases BC2, BC3 and BC5) because the wind causes waves to grow along the longest fetch in the bay. Although the wind direction for BC1 (wind speed = 5 m/s) is the same as BC2, BC3 and BC5, there is a decrease in H_s. This indicates that when the wind is not strong enough, its growing effects on waves is not enough to overcome the attenuating effects such as refraction, diffraction and bottom friction. When the wind is blowing from other directions than between N and NW, H_s continues to decrease as the waves propagate towards the head. For cases BC7 and BC9 even after passing the narrow channel close to the mouth of the bay, H_s attenuation continues at a higher rate than other cases. This is caused by the dissipation effect of the opposite directions of the wind and wave propagation. To see the percent reduction in the H_s three different points are selected, one at the mouth of the bay, one after the dissipative channel and one at the head of the bay. Table 3-2 and Table 3-3 show the coordinates of these points and the percent reduction in the significant wave height relative to the point at the mouth, respectively.

For BC1, BC2 and BC3 significant wave height maps show an increase in H_s pattern all over the bay as the wind speed increases from BC1 to BC3 (Figure 3-15). This indicates the well known wave behavior that the wind speed has a direct effect on wave generation and wave growth (Jeffreys, 1924). When the contour maps for the rest of the cases are observed, the first

difference one can notice is the locations of the areas where the H_s is less than 0.2 m (Figures 3-16 and 3-17). These calm areas exist if the wind direction is not aligned with the swell propagation direction and their locations depend mainly on the magnitude of the 'y' component of the wind. If the 'y' component dominates the wind as in cases BC7 and BC9, a low energy area is located at the SW whereas if the east component starts to dominate, this area elongates towards the NW into the islands.

Figures 3-18, 3-19 and 3-20 show mean wave direction contours that reveal the patterns of refraction. By looking at these contour maps it can be said that this final version of SWAN can predict refraction quite well even around the islands to the south of the latitude $26^{o}\ 42'\ 36''$. Since it has been observed that the SWAN wave model is capable of calculating the refraction, the contribution of the refraction to the low frequency wave attenuation will be presented in the following sections of this chapter.

Dense contours at the mouth of the bay and along the channel in average absolute wave period contour maps (Figures 3-21, 3-22, 3-23) clearly show the attenuation of low frequency waves. At the deep channel on the east side (immediately south of the bay entrance) the wave period change is not as large as it is on the west side. This may suggest that the swell attenuation is related to the depth and this will be investigated in the following sections of this chapter.

Energy dissipation (W/m^2) contour maps illustrate the sum of various processes: depth induced wave breaking, bottom friction and whitecapping (Figures 3-24, 3-25, 3-26). From these plots, it is clearly seen that a relevant cause of significant wave height attenuation and average mean period maps is energy dissipation. It is possible to see the high correspondence of energy dissipation with H_s and average mean period especially at the locations where strong attenuation occurs. For example, at the bay entrance, where water depth decreases by 6 m, it is possible to

observe higher rates of energy dissipation and significant wave height. It should also be noted that the reduction in the depth here may also have a contribution to the swell attenuation.

After determination of the correspondence between energy dissipation and significant wave height attenuation, three more cases were run to observe the effect of bottom friction, wave induced breaking and whitecapping to the significant wave height and the wave spectra. New cases were generated by changing the dissipation formulations of the base case, BC2, without changing the bathymetry, wave and wind conditions. In the first case bottom friction was reduced by introducing a very small coefficient into the JONSWAP formulation ([cfjon] = 0.0001 m^2/s^3) to be able to see the contribution of bottom friction to the low frequency wave attenuation. For the second case the coefficient of JONSWAP formulation was kept at 0.0001 m^2/s^3 and in the mean time, the depth–induced wave breaking option of SWAN was turned off. Finally, for the third case whitecapping was turned off in addition to the conditions in case 2. These three cases were compared with the base case, BC2, and the maximum differences of significant wave height and energy dissipation between the new cases and BC2 are displayed in Table 3-4. These results showed that the greatest difference occurred at the shallow section of the bay entrance (especially over the sand bar). The most significant contribution to energy dissipation was from bottom friction with a value of 16.636 W/m^2 and this caused the highest attenuation in H_s with a value of 3.02 m. According to the results presented in Table 3-4 depth–induced wave breaking and whitecapping do not have a significant effect on the energy dissipation. As a matter of fact it is possible to see the greatest effects of depth–induced breaking at the breaking zone. However, for the purpose of this study data at the breaking zone was not examined. Although it was possible to observe the differences in energy dissipation and H_s due to bottom friction, depth–induced wave breaking and whitecapping separately, Figure 3-27

shows that these factors do not affect the wave spectra significantly. It only shows the spectra for the base case, BC2, and the case without bottom friction, depth–induced wave breaking and whitecapping. Even in this case, the spectra for these cases are almost identical and this suggests that attenuation (or energy dissipation) of the waves as they propagate towards the head is not greatly affected by bottom friction, depth–induced breaking or whitecapping.

The previous test showed that the attenuation of the low frequency waves was not affected significantly by the components of energy dissipation. Additional reasons for the low frequency waves to attenuate can be the refraction and shoaling. Since both refraction and shoaling are depth–dependent occurrences, some changes were made on the bathymetry file to observe the change in the behavior of the low frequency waves. For this purpose, three new cases were run with a wind velocity and wave forcing the same as the base case, BC2, but with flat bathymetries of depths 2, 25, 50 and 100 m. It should be noted that the JONSWAP friction coefficient, depth–induced breaking and whitecapping options were not changed or turned off for the new cases. Depths were chosen to be able to observe the behavior of the bay in shallow, intermediate and deep water conditions. Waves can be categorized as shallow water waves, intermediate depth waves and deep water waves according to the following conditions (Dean and Dalrymple, 1991):

$(kh) > \frac{\pi}{10}$ Shallow Water Waves

$\frac{\pi}{10} < (kh) < \pi$ Intermediate Depth Waves

$(kh) < \pi$ Deep Water Waves

where k is the wave number and h is the water depth.

Using these conditions, a wave period of 10 s (wave period selected for model calculations) and the dispersion relationship, $\sigma^2 = (gk)\tanh(kh)$, where g is the gravitational acceleration, one can obtain the depths separating shallow water from intermediate depth and intermediate depth from deep water. These depths were found to be 2.38 and 77.87 m, respectively. Figures 3-28 and 3-29 show the one dimensional wave spectra for these cases. The plot for 2 m represents shallow water waves, plots for 25 and 50 m represent intermediate depth and 100 m represents deep water conditions. From these figures it is possible to observe that low frequency waves can propagate further into the bay as the water depth increases (i.e. as the waves propagate in deeper water). For instance, for shallow water (depth of 2 m), 10 s waves cannot be observed after 500 m into the bay from the mouth, but for intermediate depths of 25 and 50 m, it is possible to observe them up to 20 km. On the other hand one may expect to observe low frequency waves further into the bay for the deep water case. However, model results showed that even for a depth of 100 m low frequency waves disappeared 22 km before reaching the head. Because bathymetric effects were eliminated by introducing a flat bottom, and hence refraction effects were suppressed, one possible reason for the wave dissipation was the geometry of the bay. The bay did not have a straight geometry causing waves to be blocked as they propagate, especially at latitudes $26^{o}\ 42'\ 36''$ and $26^{o}\ 46'\ 48''$. At locations where the propagation of low frequency waves was blocked, energy was distributed laterally, perpendicular to the dominant wave direction and thus waves attenuated. This phenomenon is called wave diffraction (Dean and Dalrymple, 1991). The version of SWAN that was used for this study has the ability to consider the effects of diffraction and in this particular case, since the bathymetric effects were eliminated, it may be possible to observe diffraction effects. However, since diffraction is more effective in small-scale models, one other case was added to verify the effects of diffraction. In

this case diffraction was eliminated from the base case, BC2, and wave spectra are presented in Figure 3-30. As the figures suggest, diffraction affects swell waves at the mouth of the bay where dimensions are relatively smaller than the rest of the bay. However, its effect decreases as the waves propagate into the bay and hence it is not possible to observe swell waves beyond 16 km.

Since it is not possible to observe swell waves at the head of the bay even after eliminating bottom friction, refraction and diffraction, one final case is added to be able to observe the effect of bay geometry. In this case, the bay geometry was replaced by a rectangle with a width of 7 km and a length of 42 km. Once again a flat bottom in deep water conditions (100 m) was selected and waves were prescribed to propagate southward from the north boundary of the bay with a wave height of 1.5 m and wave period of 10 s. Wave propagation direction was changed for this case to be able to make the propagation direction perpendicular to the bottom contours. In addition to these, bottom friction was reduced once again by assigning the coefficient of JONSWAP to be 0.0001 m^2/s^3. Figure 3-31 shows the wave spectra for this case and as it can be observed from the figure, some low frequency waves were able to propagate from the mouth to the head without attenuation.

Figure 3-32 shows the distribution of the wave spectra along the distance from the bay mouth to the head, at a wave frequency of 0.1 Hz for the cases BC2; BC2 without bottom friction, depth–induced breaking and whitecapping; flat bottom with a water depth of 100 m; and rectangular bay without bottom friction, depth–induced breaking and whitecapping. With the original bay geometry, even for the most basic case where bottom friction, depth-induced breaking, whitecapping, refraction and diffraction were eliminated, energy density curve decreases from mouth to the head. However, when bay is replaced with a rectangle with the same dimensions, wave energy kept constant. This shows that most of the swell waves could not reach

the head of the bay because of the blocking effect of the land. In addition, it has been observed that diffraction, bottom friction, whitecapping and depth-induced breaking have very small contribution to swell attenuation. Refraction has the most contribution to the swell attenuation, especially close to the bay mouth where waves had not been blocked by the land. The contributions of refraction, diffraction and the combined effect of bottom friction, whitecapping and depth-induced breaking were calculated from the areas under the energy density curves and are represented in Table 3-5. This table shows most of the contribution to the swell attenuation is caused by refraction close to the mouth and the effect of diffraction, bottom friction, depth–induced breaking and whitecapping is negligibly small.

Table 3-1 Coordinates of the points where the frequency spectra is obtained

X – Coordinate (m)	Y – Coordinate (m)
7769.3599	41578.6016
8584.3398	39341.1992
9562.3301	36637.6992
10540.2998	33561.1992
11681.2998	31417.0000
12278.9004	29366.0000
12604.9004	27315.0000
12713.5996	25543.6992
13039.5996	22747.0000
13256.9004	20416.3008
14180.5996	18458.5000
14886.9004	16966.9004
15484.5996	15195.5996
16625.5000	13610.7998
17657.9004	12305.5996
18472.8008	10441.0996
19831.0996	8483.3398
21352.5000	6432.3701
22765.0996	4101.7100
24014.6992	1491.3800

Table 3-2 Coordinates of significant wave height observation points

	Point at the Mouth	Point after the channel	Point at the head
Longitude	-111.8781	-111.8398	-111.7208
Latitude	26.8835	26.7807	26.5608

Table 3-3 Percent reduction in significant wave height

	% REDUCTION IN SIGNIFICANT WAVE HEIGHT	
Test Cases	Point after the channel	Point at the head
BC1	70.53	72.80
BC2	43.62	39.32
BC3	31.88	20.76
BC4	47.71	47.95
BC5	53.64	45.71
BC6	57.97	60.01
BC7	52.59	91.49
BC8	52.60	58.23
BC9	48.33	94.64

Table 3-4 Differences in H_s and energy dissipation for the cases without bottom friction (Case 1); without bottom friction and depth induced wave breaking (Case 2); and without bottom dissipation, depth induced wave breaking and whitecapping (Case 3).

Difference Between	Max. Difference in Energy Dissipation (W/m^2)	Max. Difference in Hs (m)
Case 1 and BC2	16.621	3.020
Case 2 and BC2	16.636	3.051
Case 3 and BC2	16.639	3.069

Table 3-5 Percent reduction in energy per unit wave ray length due to combined effects of bottom friction, depth-induced breaking and whitecapping; refraction and diffraction.

Attenuation due to	% Reduction in Energy
Refraction	14
Combined effect of bottom friction, depth-induced breaking and whitecapping	< 1
Diffraction	< 1
Blocking of land	84

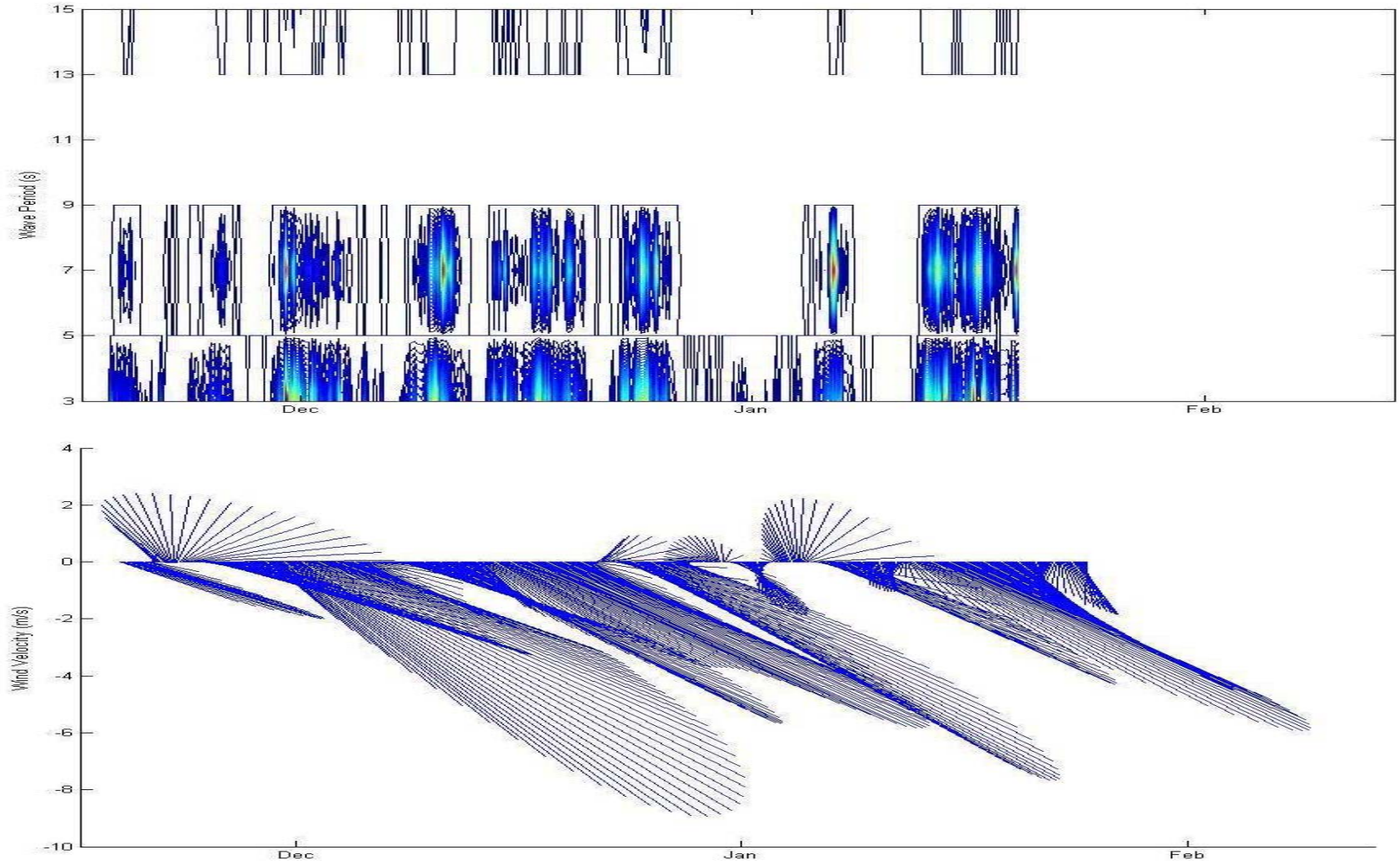

Figure 3-1 Wave Energy Contours and Wind Velocity Vectors at ST1 between November 2004 and February 2005

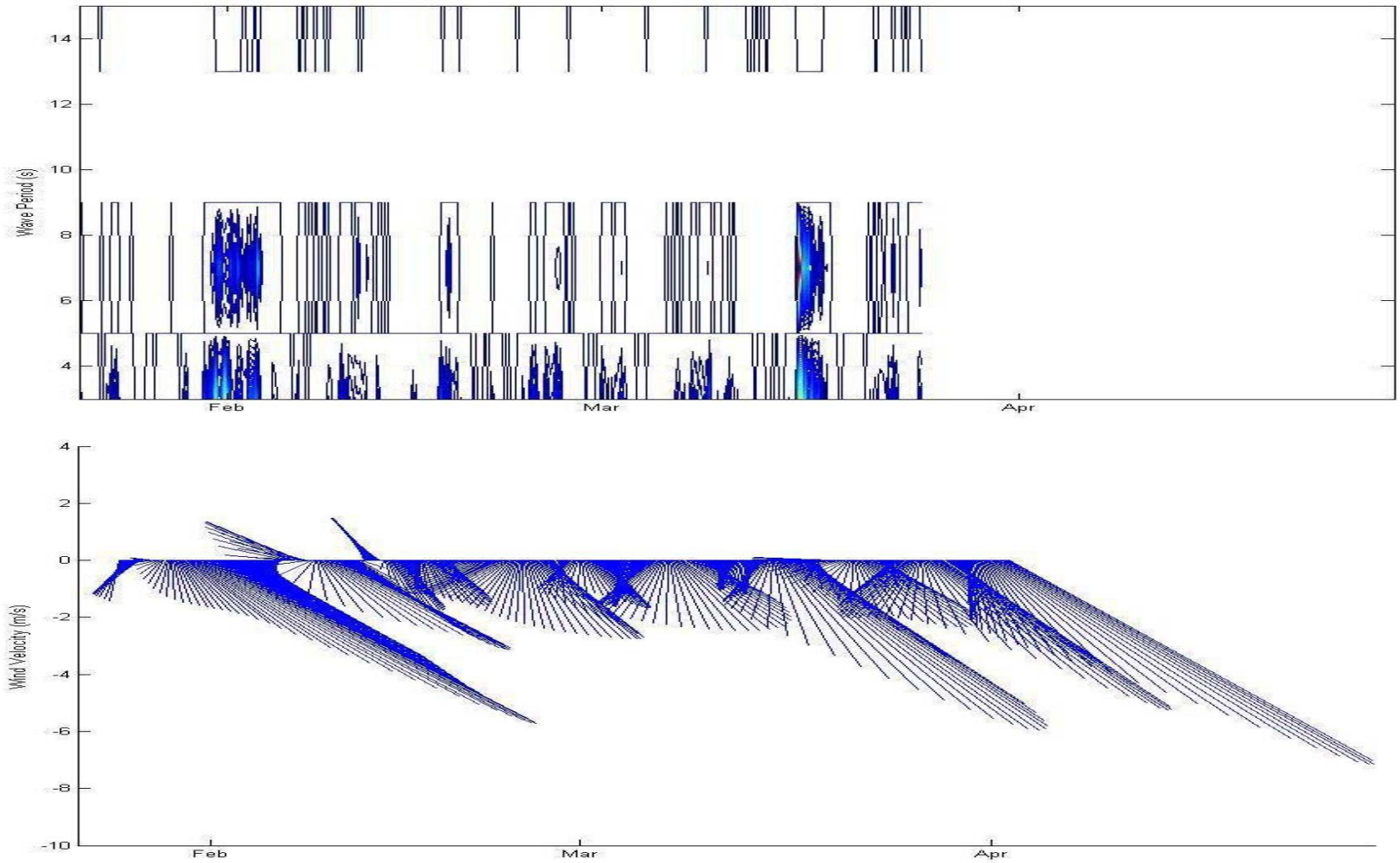

Figure 3-2 Wave Energy Contours and Wind Velocity Vectors at ST1 between February 2005 and April 2005

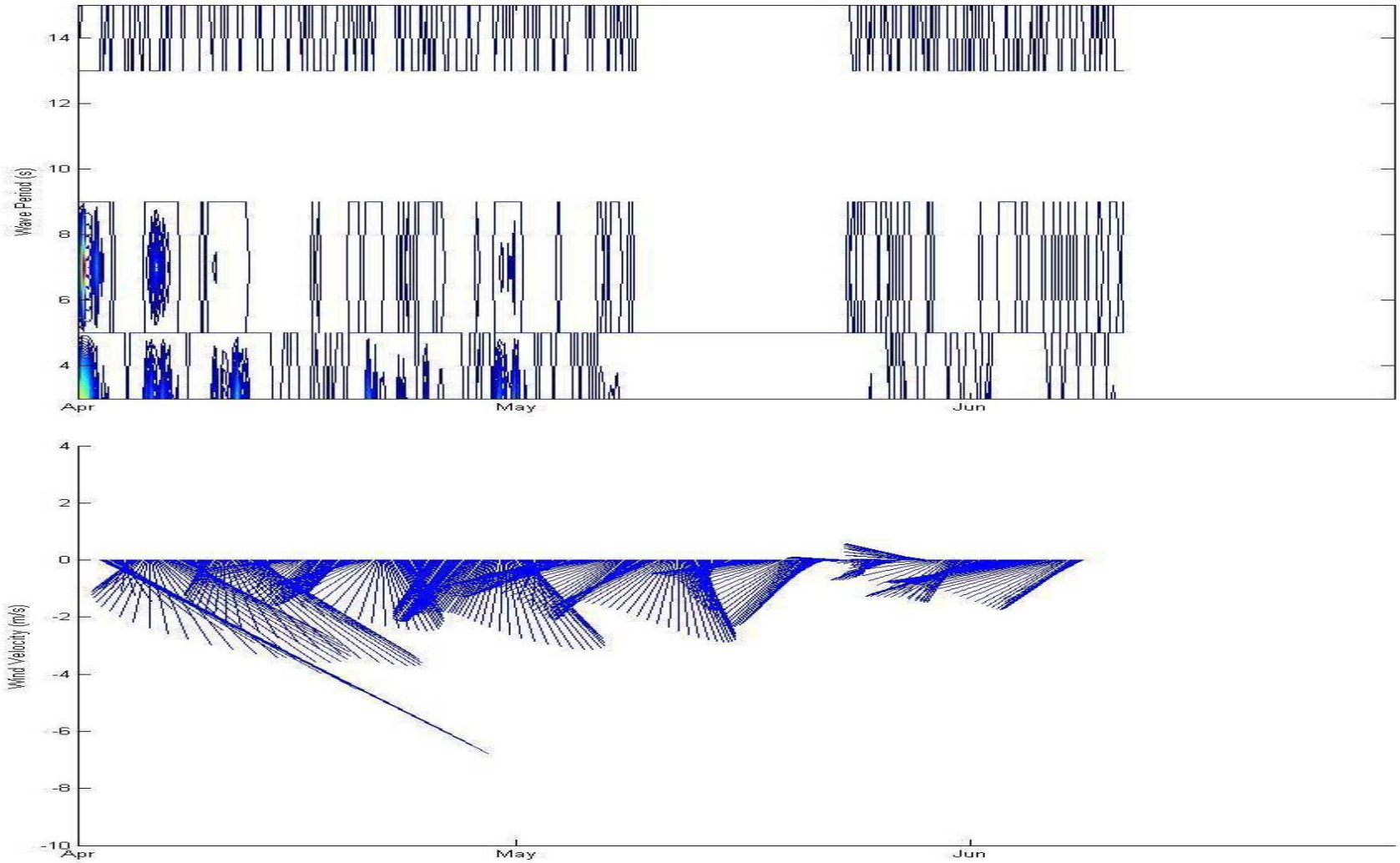

Figure 3-3 Wave Energy Contours and Wind Velocity Vectors at ST1 between April 2005 and June 2005

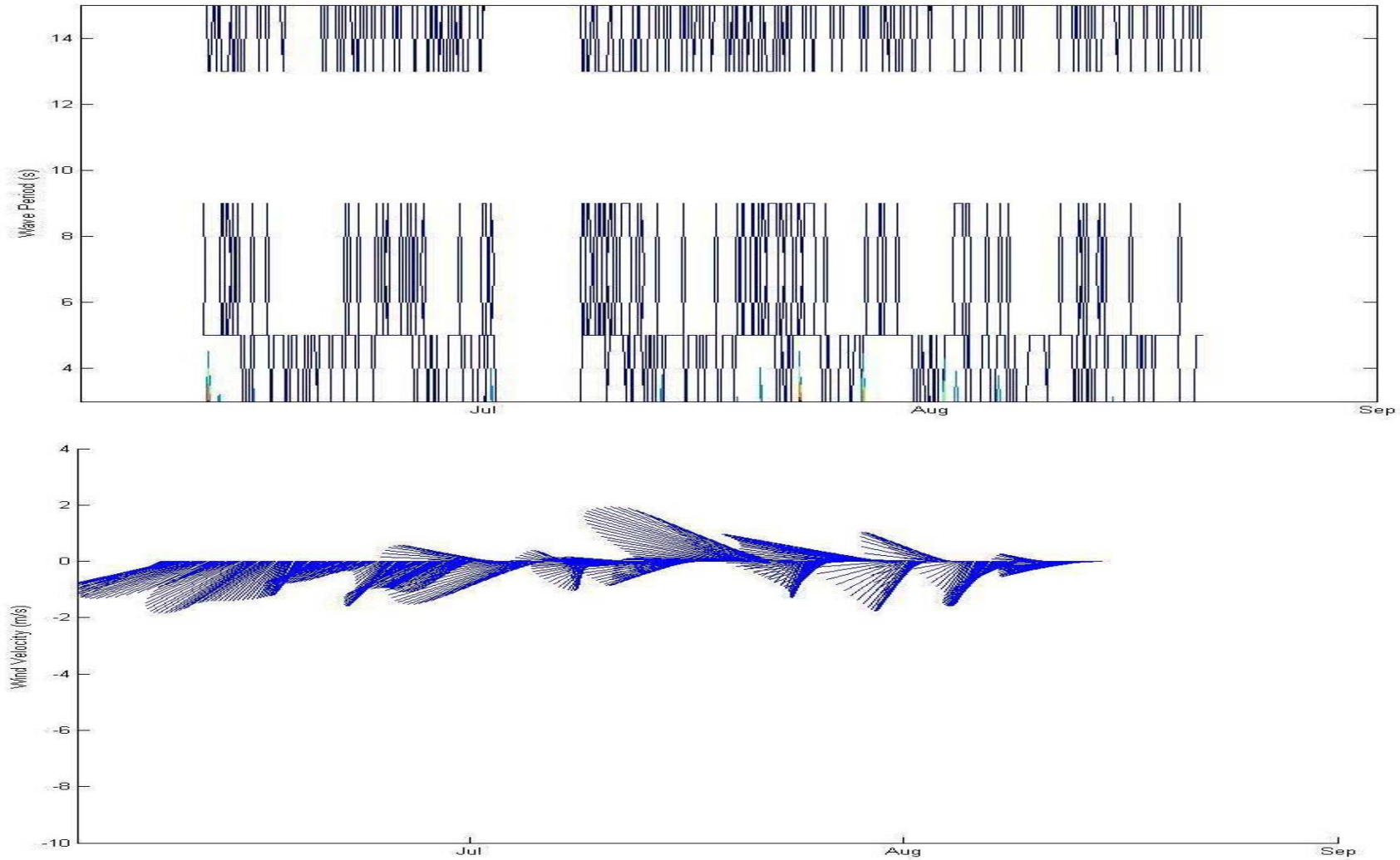

Figure 3-4 Wave Energy Contours and Wind Velocity Vectors at ST1 between June 2005 and August 2005

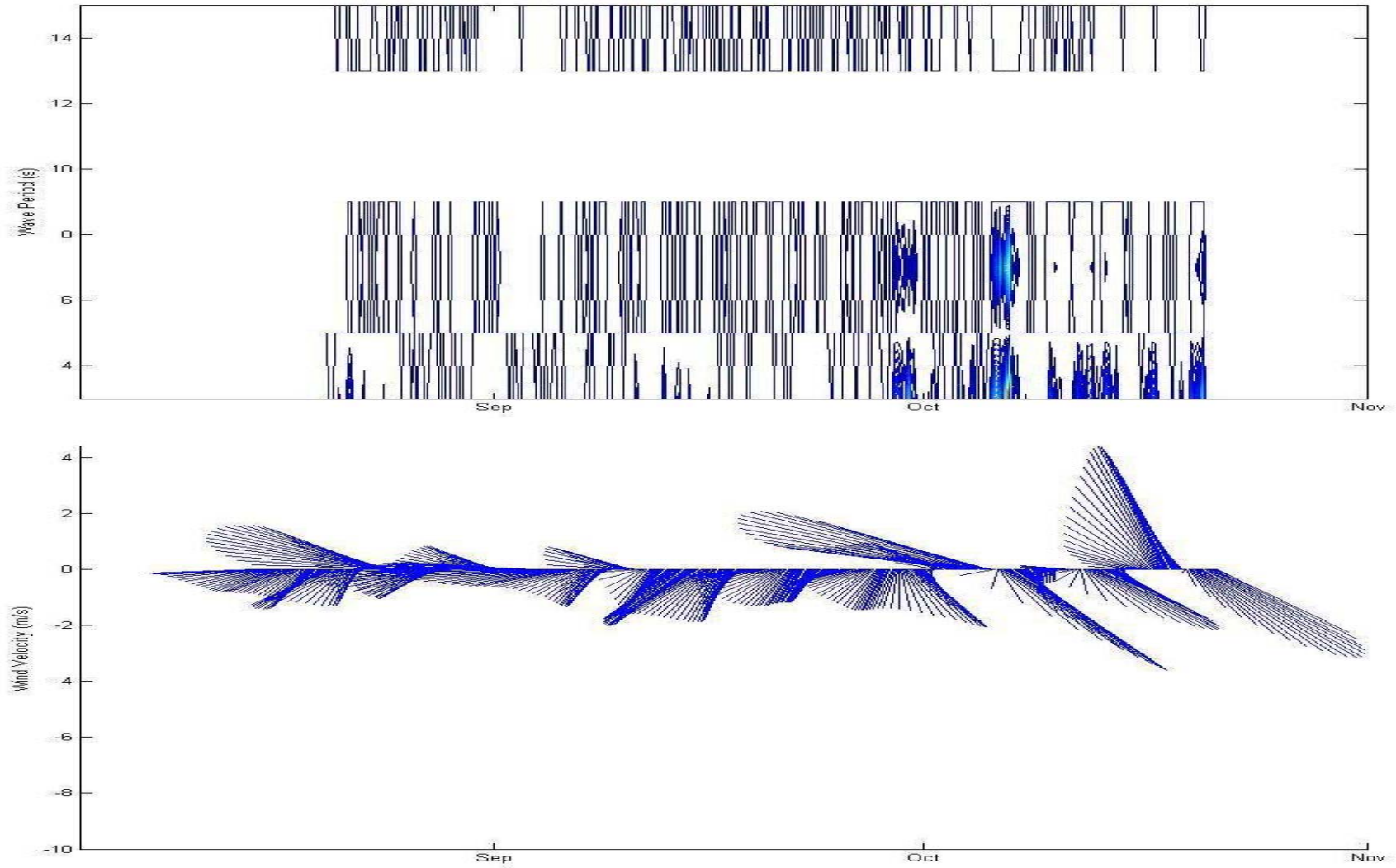

Figure 3-5 Wave Energy Contours and Wind Velocity Vectors at ST1 between August 2005 and November 2005

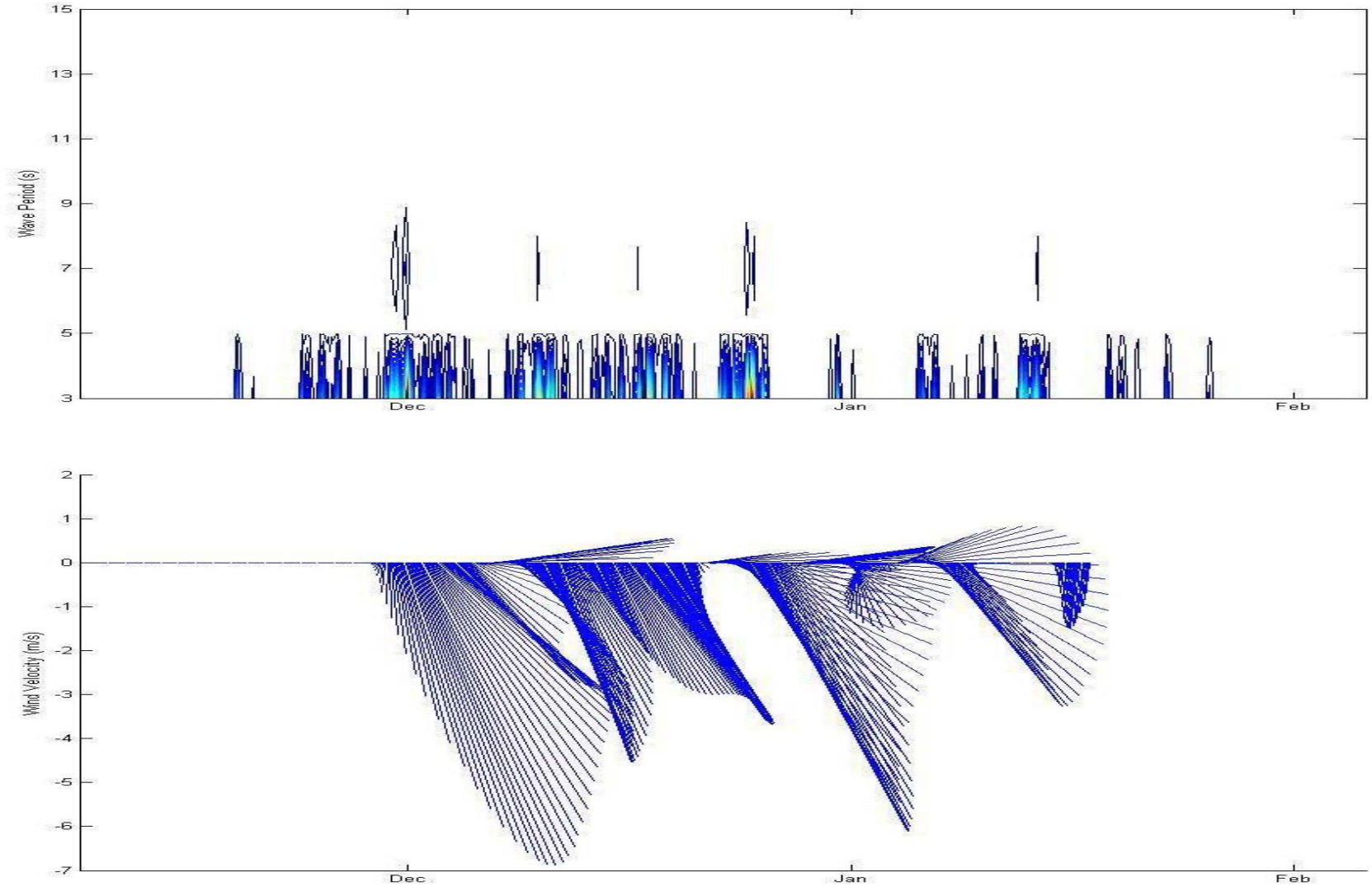

Figure 3-6 Wave Energy Contours and Wind Velocity Vectors at ST2 between November 2004 and February 2005

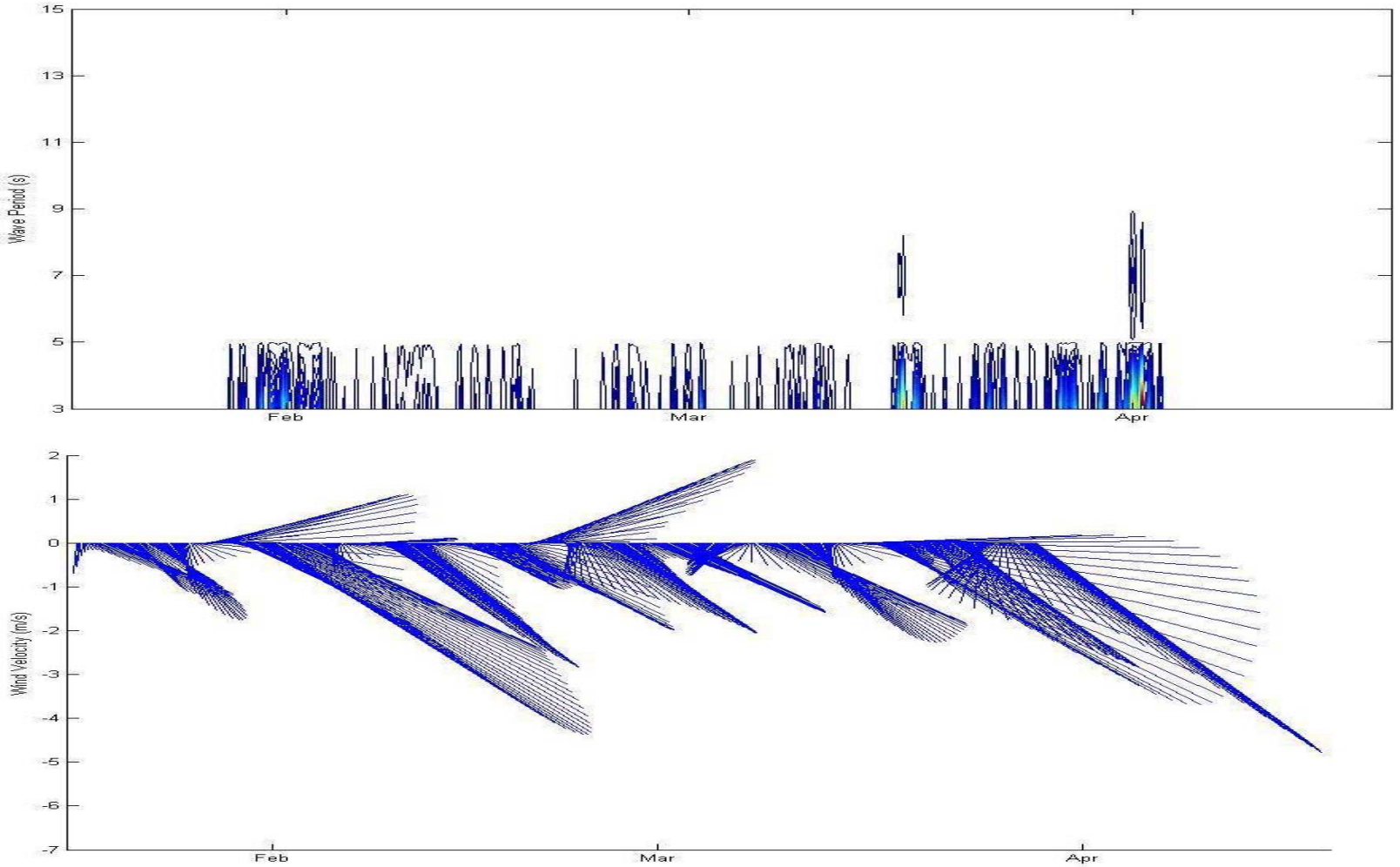

Figure 3-7 Wave Energy Contours and Wind Velocity Vectors at ST2 between February 2005 and April 2005

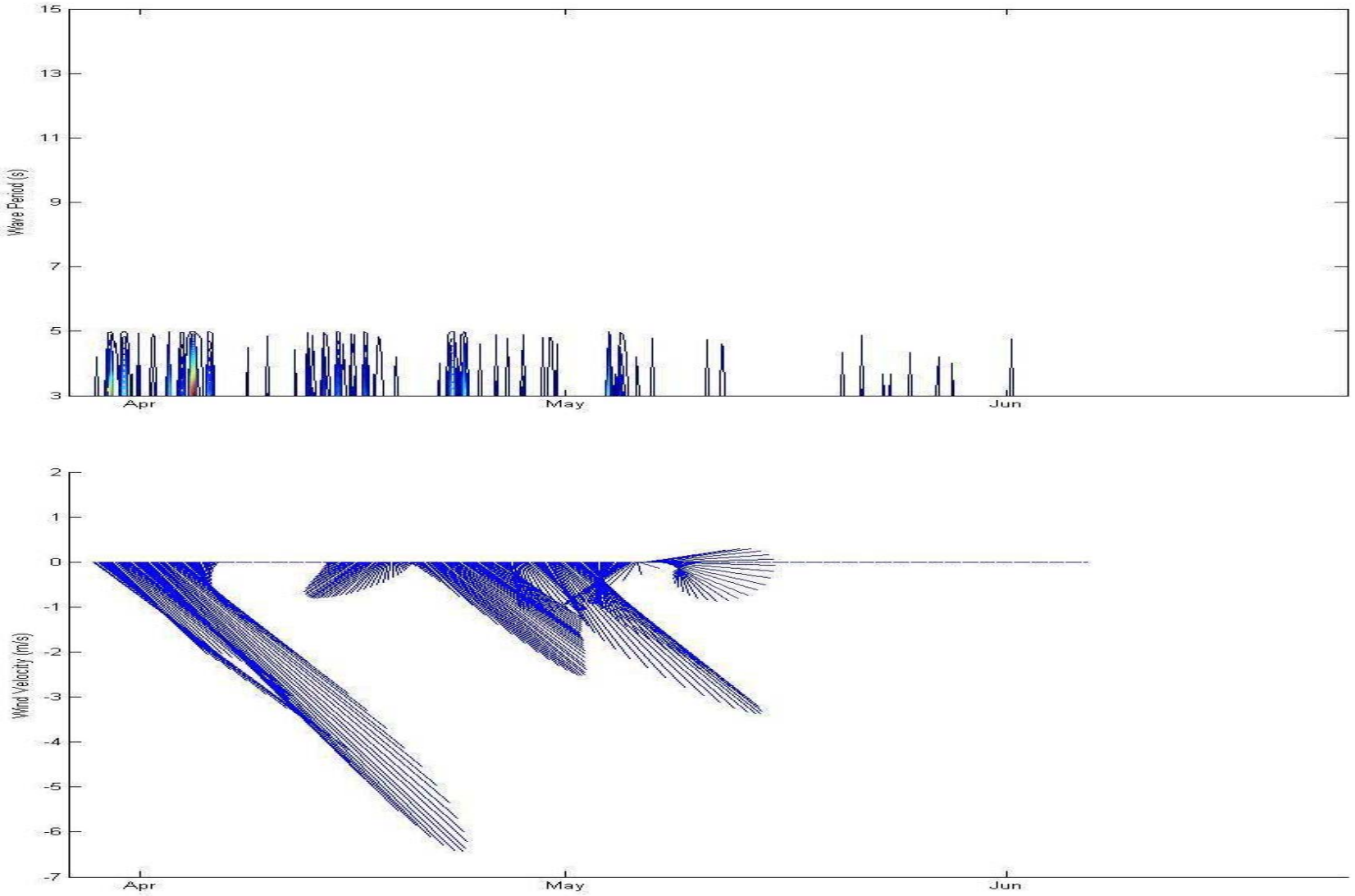

Figure 3-8 Wave Energy Contours and Wind Velocity Vectors at ST2 between April 2005 and June 2005

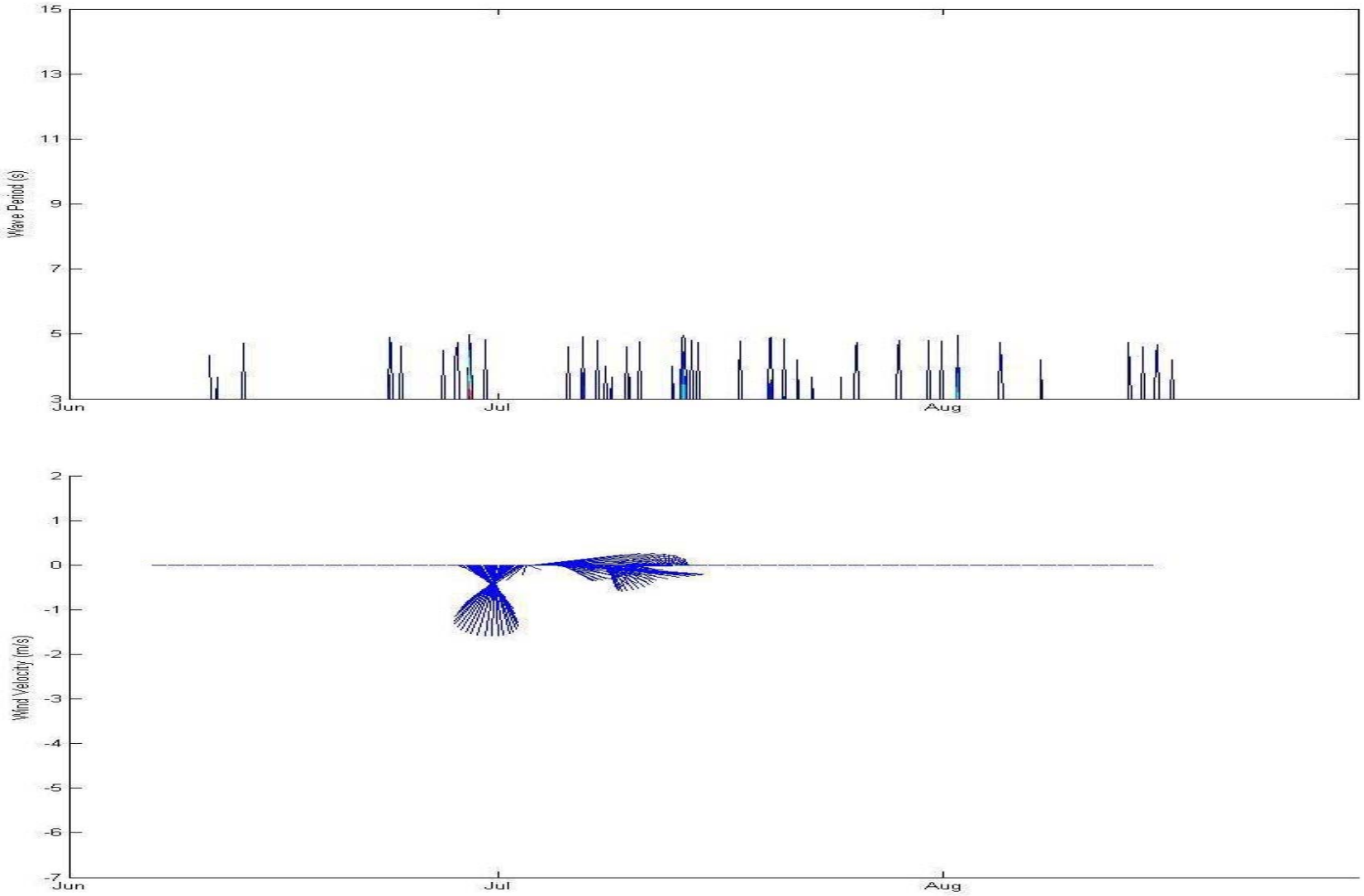

Figure 3-9 Wave Energy Contours and Wind Velocity Vectors at ST2 between June 2005 and August 2005

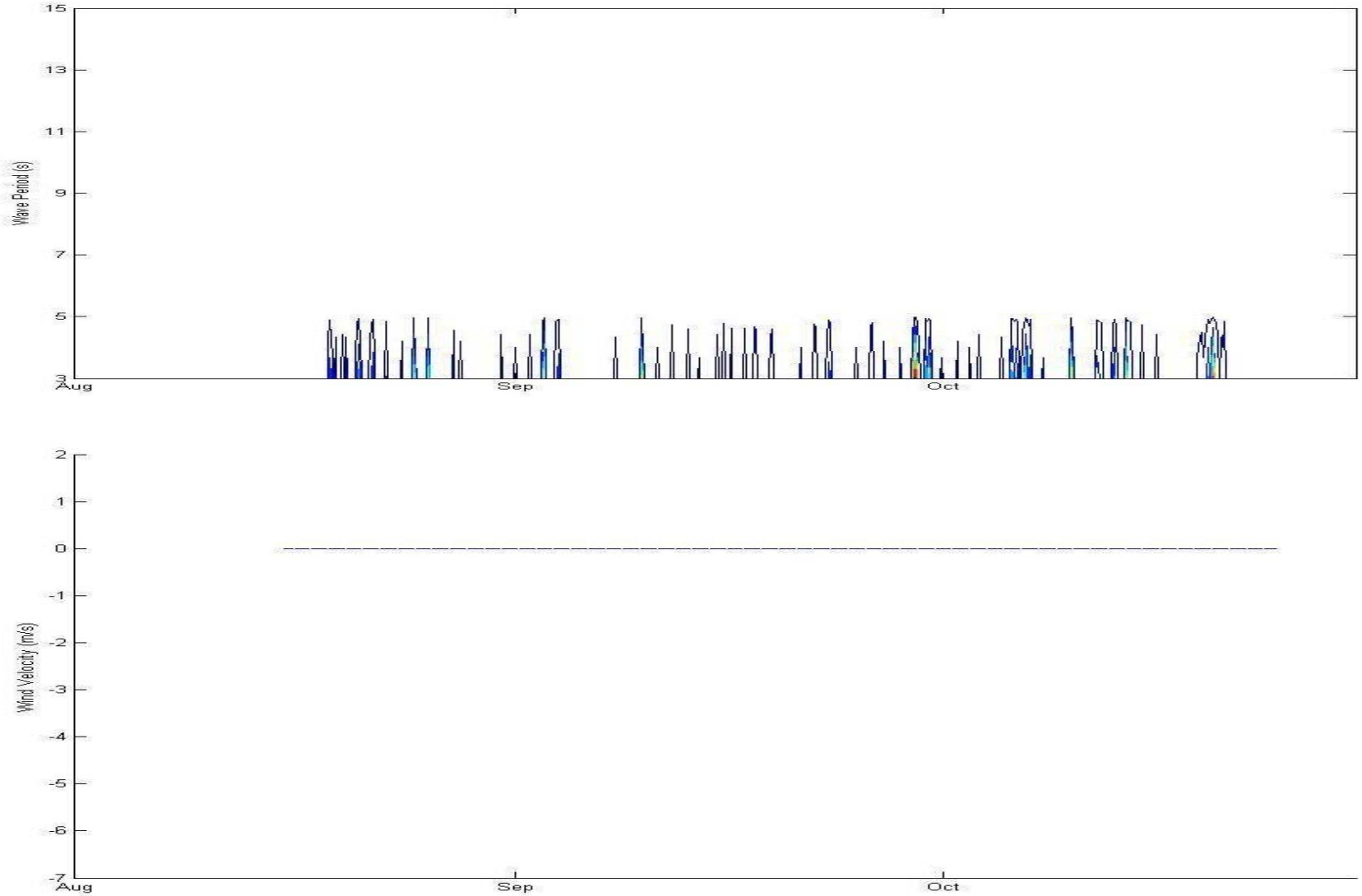

Figure 3-10 Wave Energy Contours and Wind Velocity Vectors at ST2 between August 2005 and November 2005

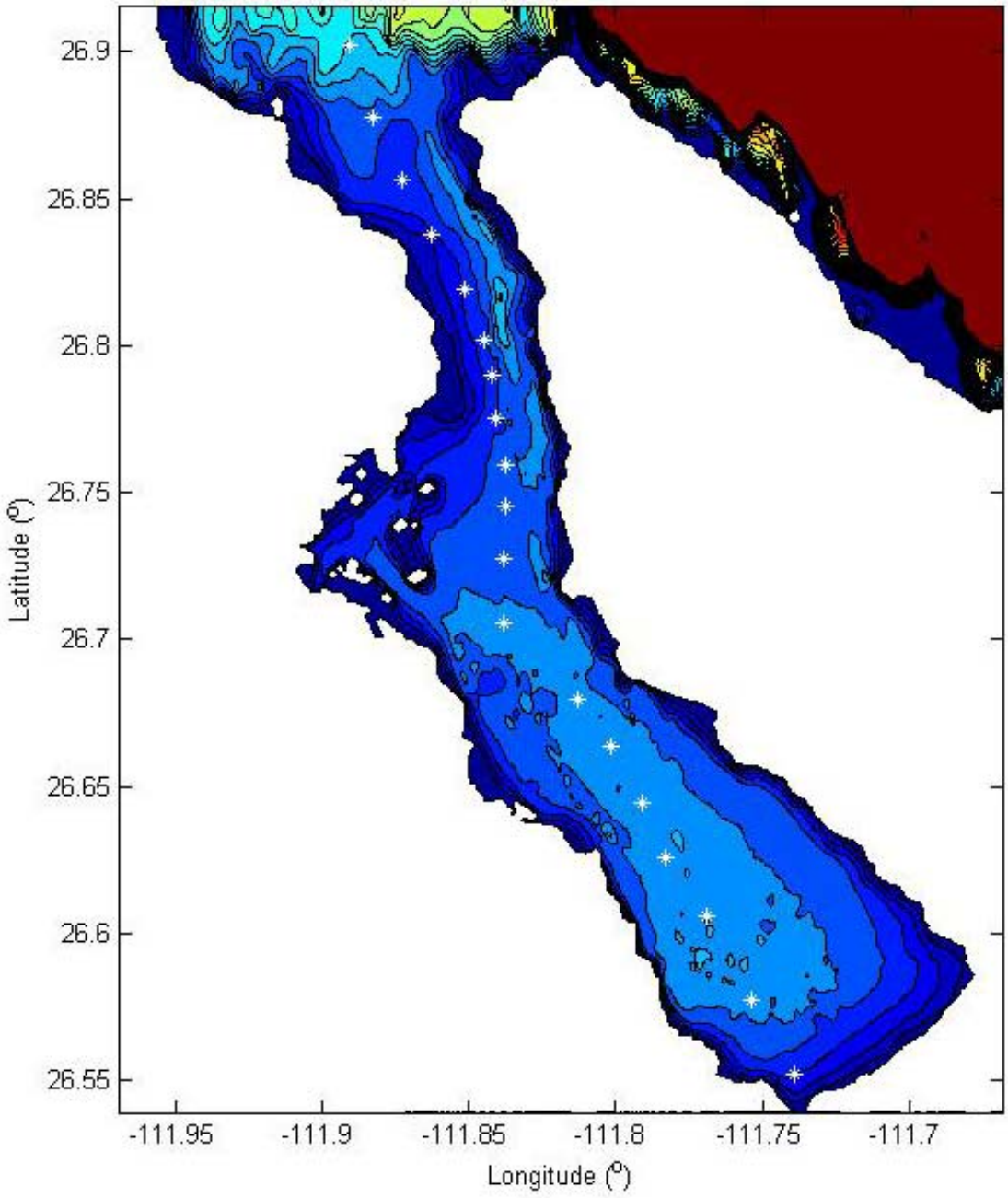

Figure 3-11 Graphical Representation of the Points where 1D Wave Spectra was Requested

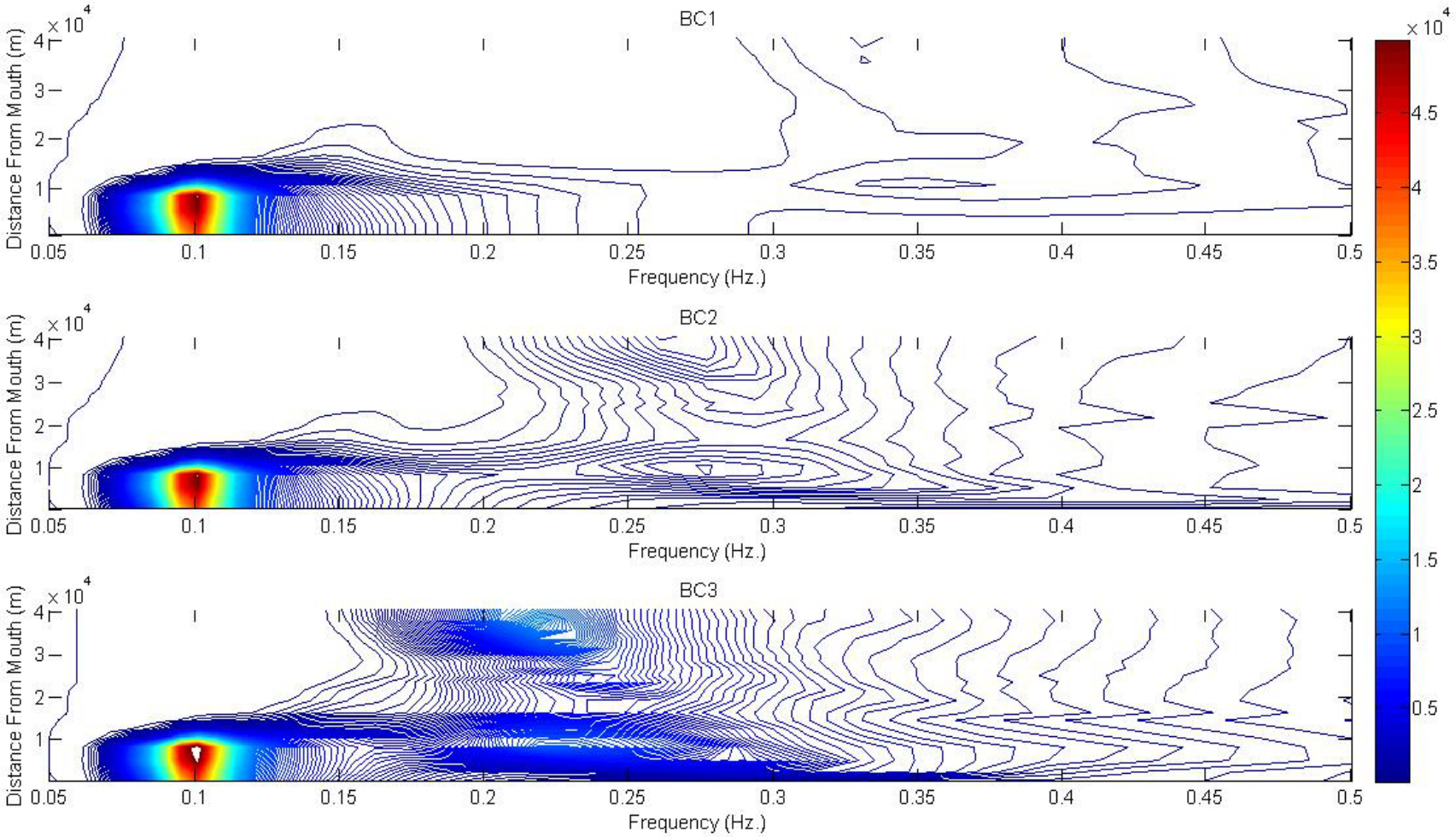

Figure 3-12 Spatial Energy Density Contours in J/m^2 for BC1, BC2 and BC3

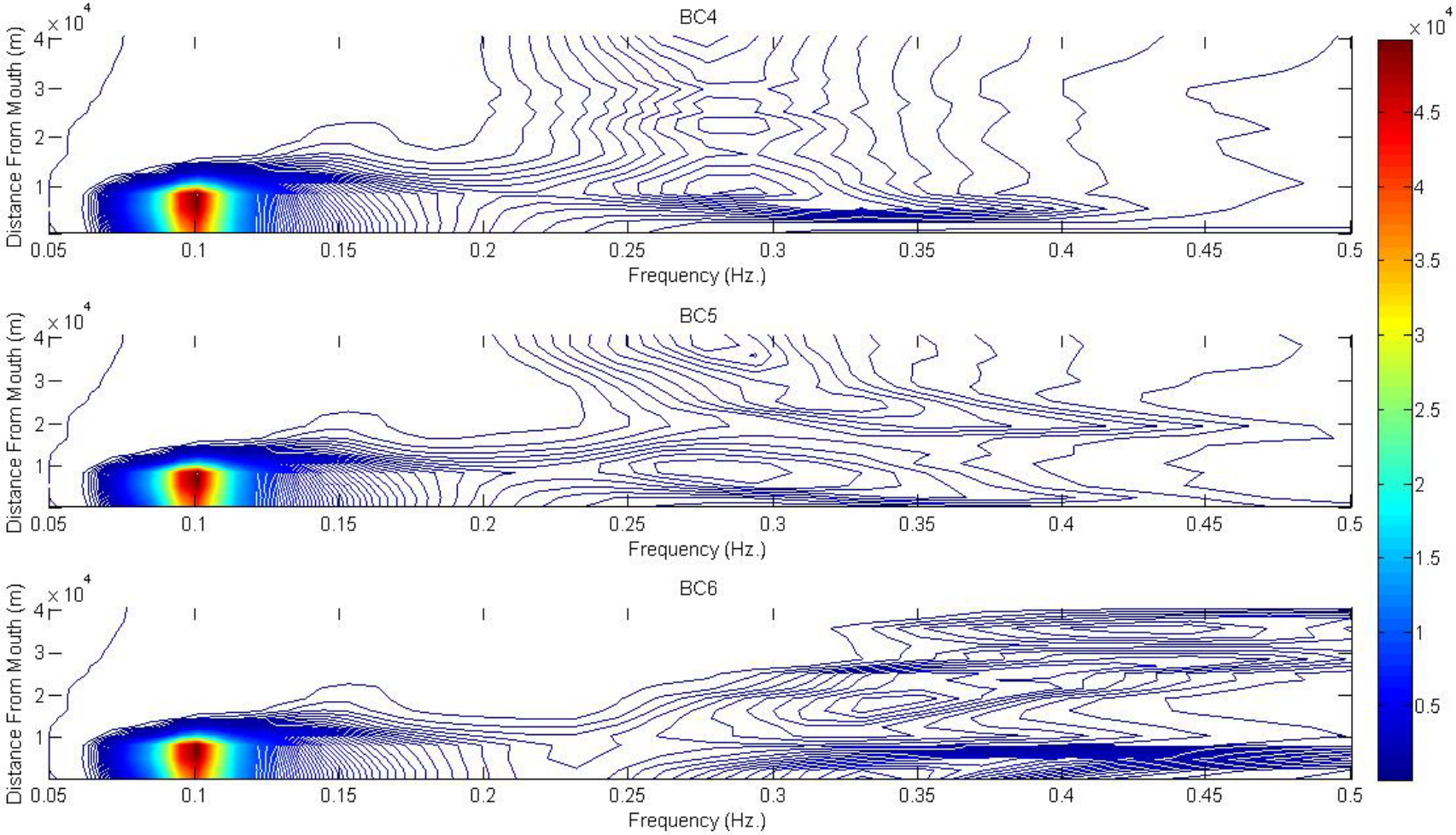

Figure 3-13 Spatial Energy Density Contours in J/m^2 for BC4, BC5 and BC6

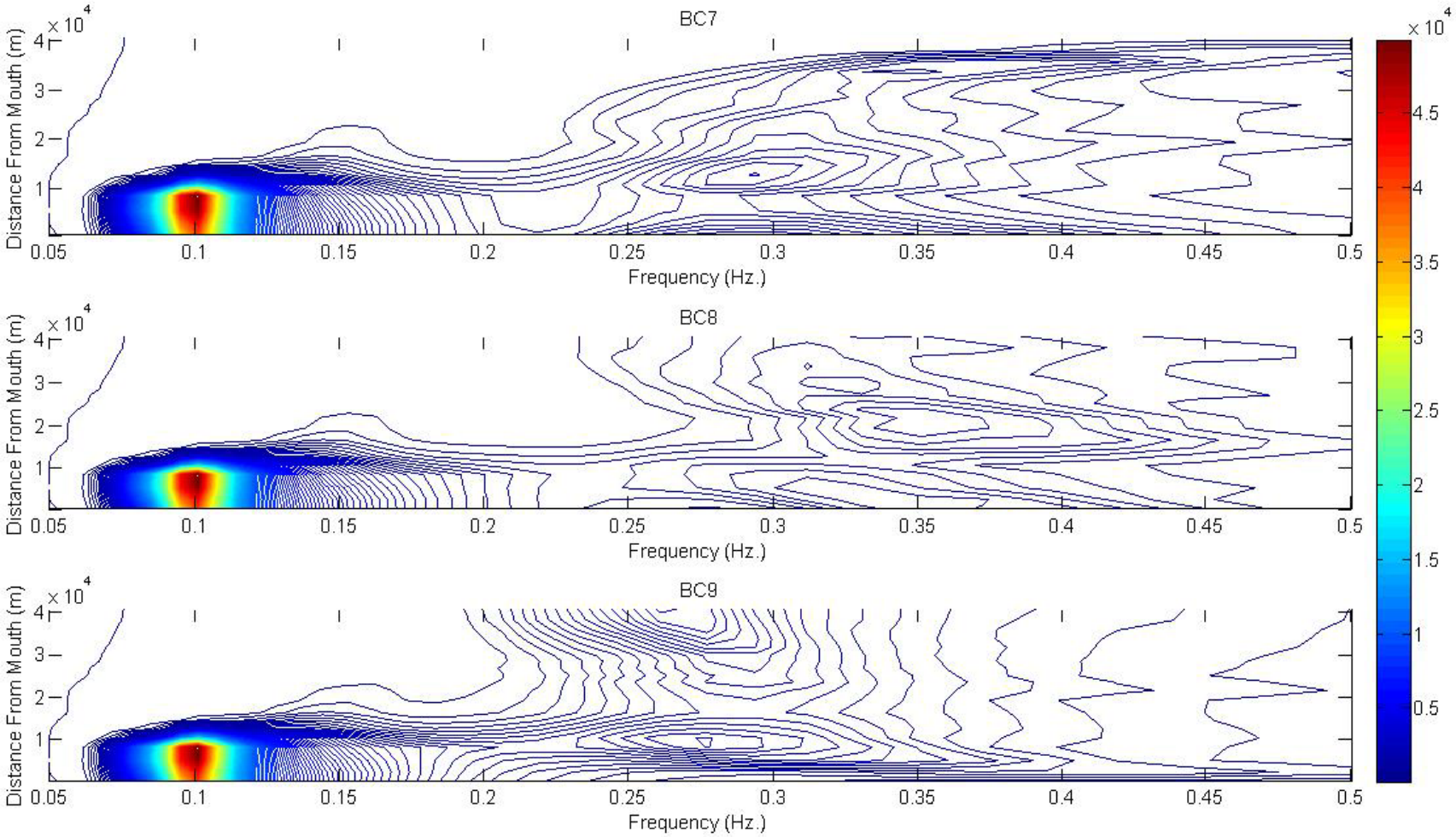

Figure 3-14 Spatial Energy Density Contours in J/m^2 for BC7, BC8 and BC9

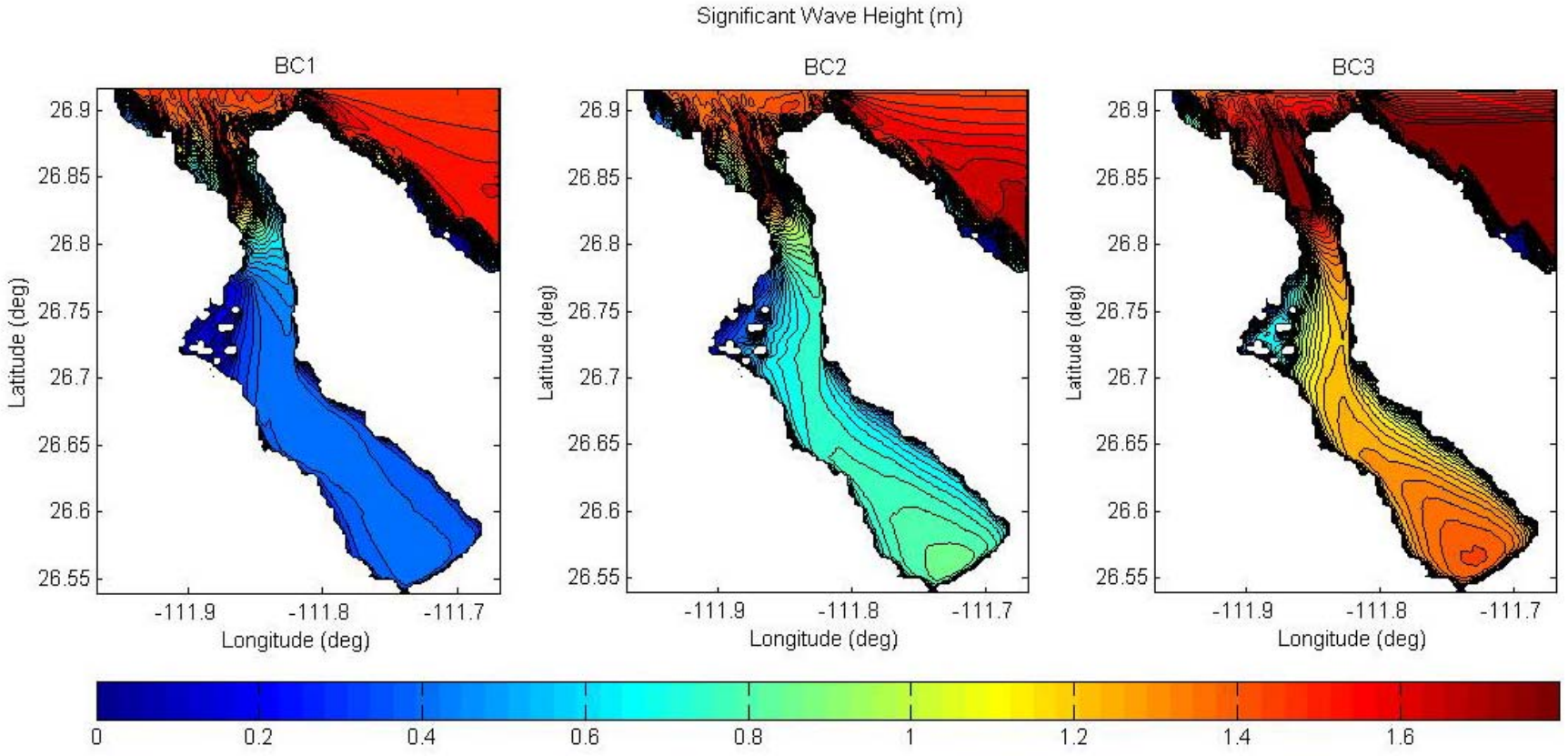

Figure 3-15 Significant Wave Height Contours for BC1, BC2 and BC3

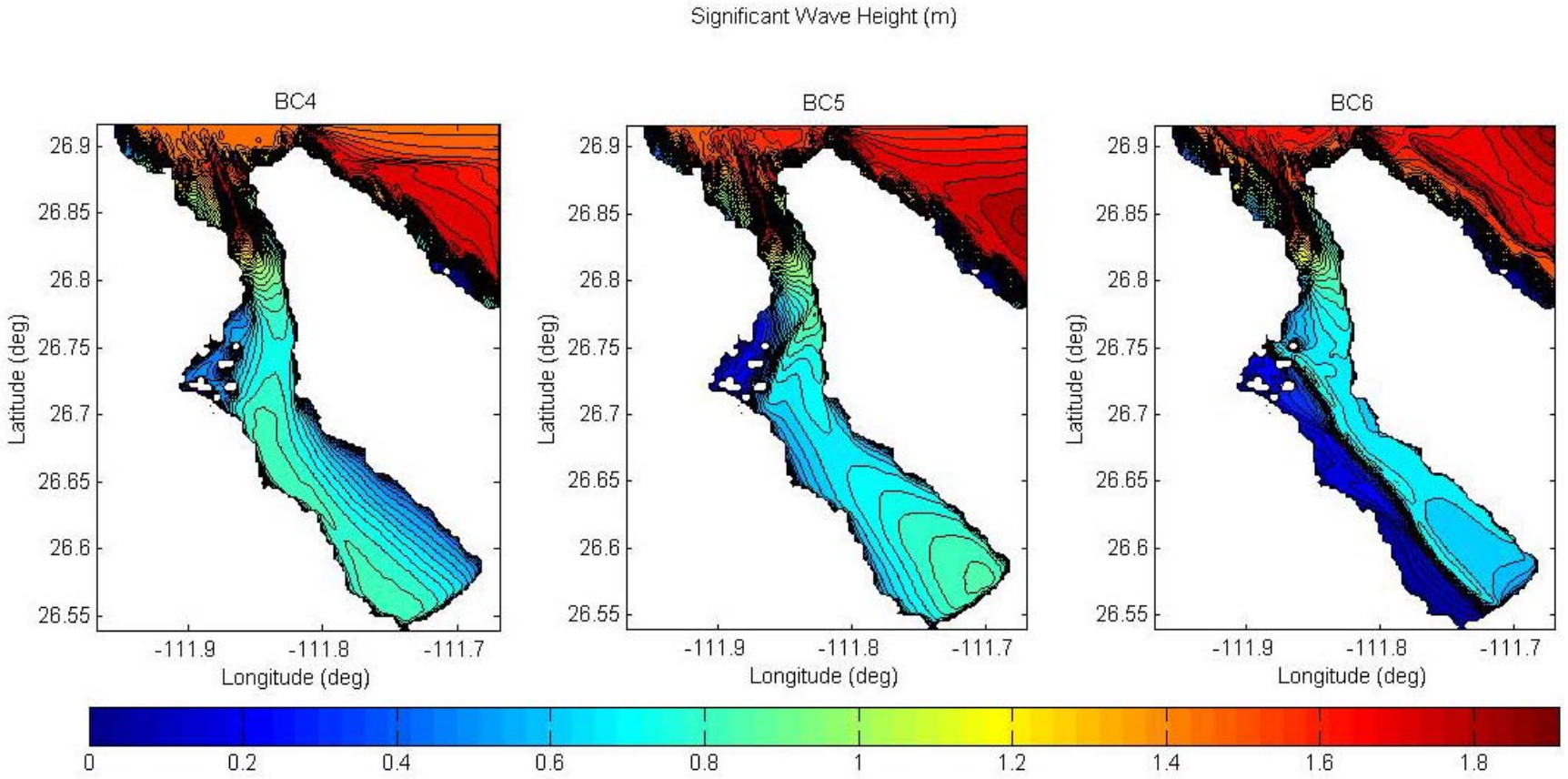

Figure 3-16 Significant Wave Height Contours for BC4, BC5 and BC6

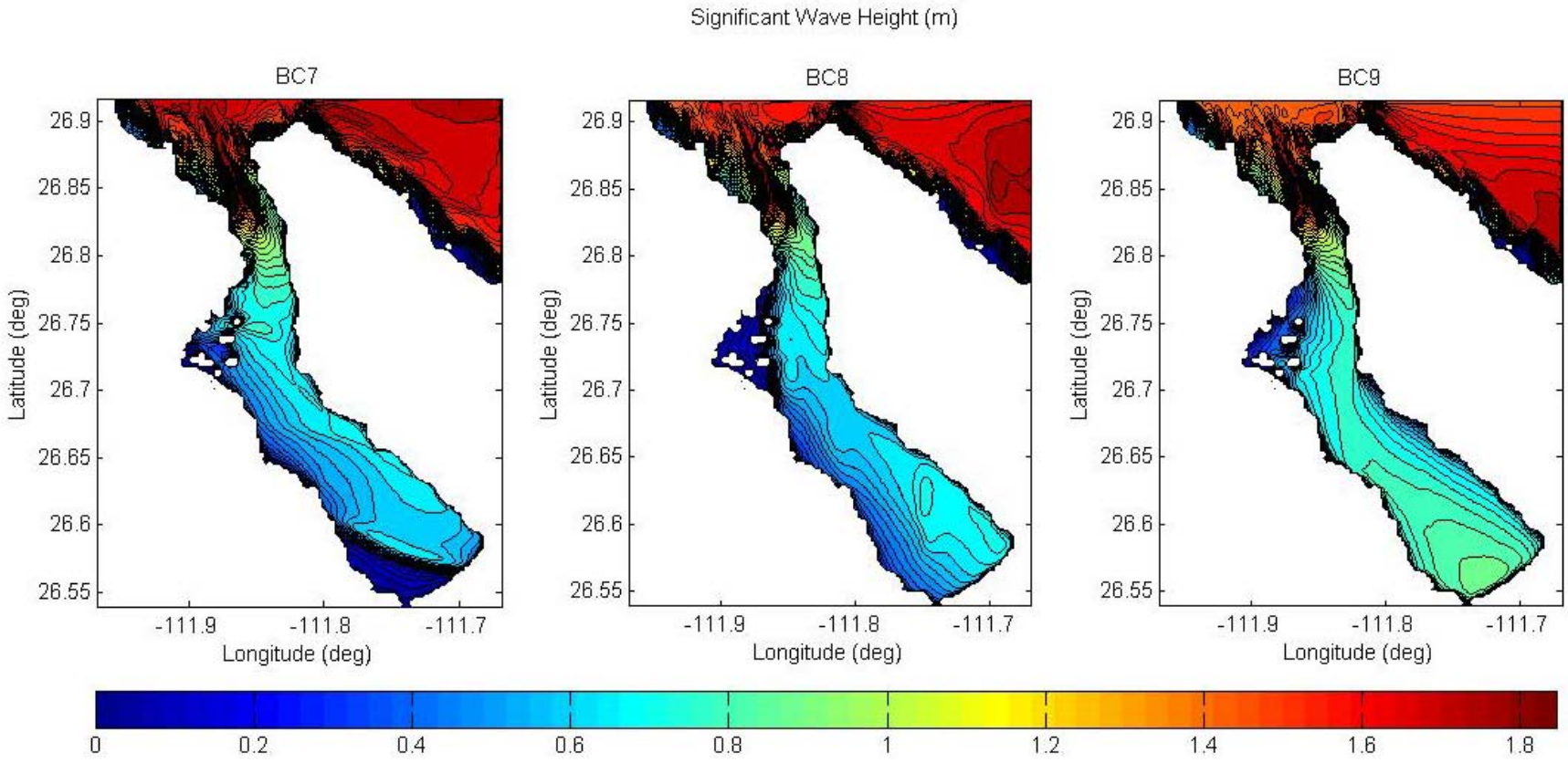

Figure 3-17 Significant Wave Height Contours for BC7, BC8 and BC9

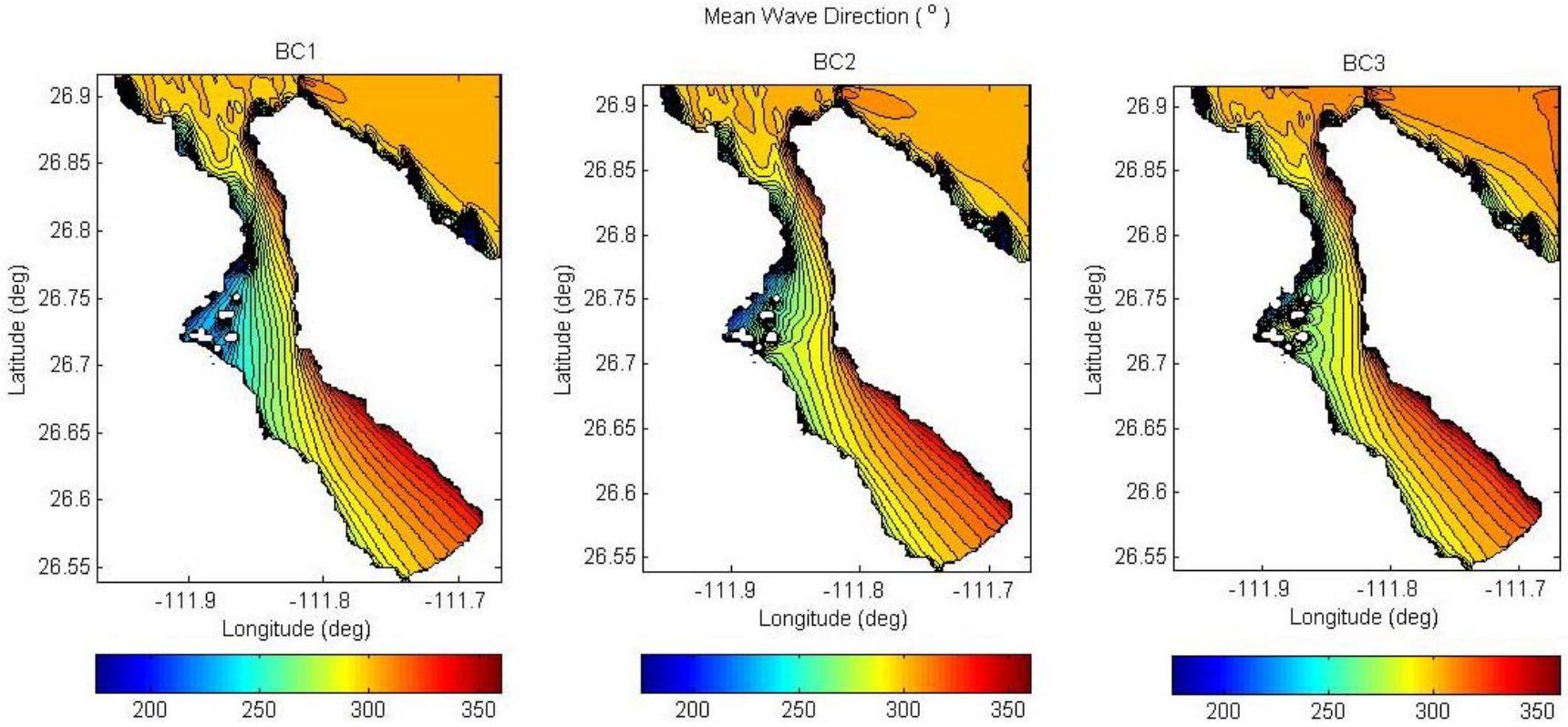

Figure 3-18 Mean Wave Direction Contours for BC1, BC2 and BC3

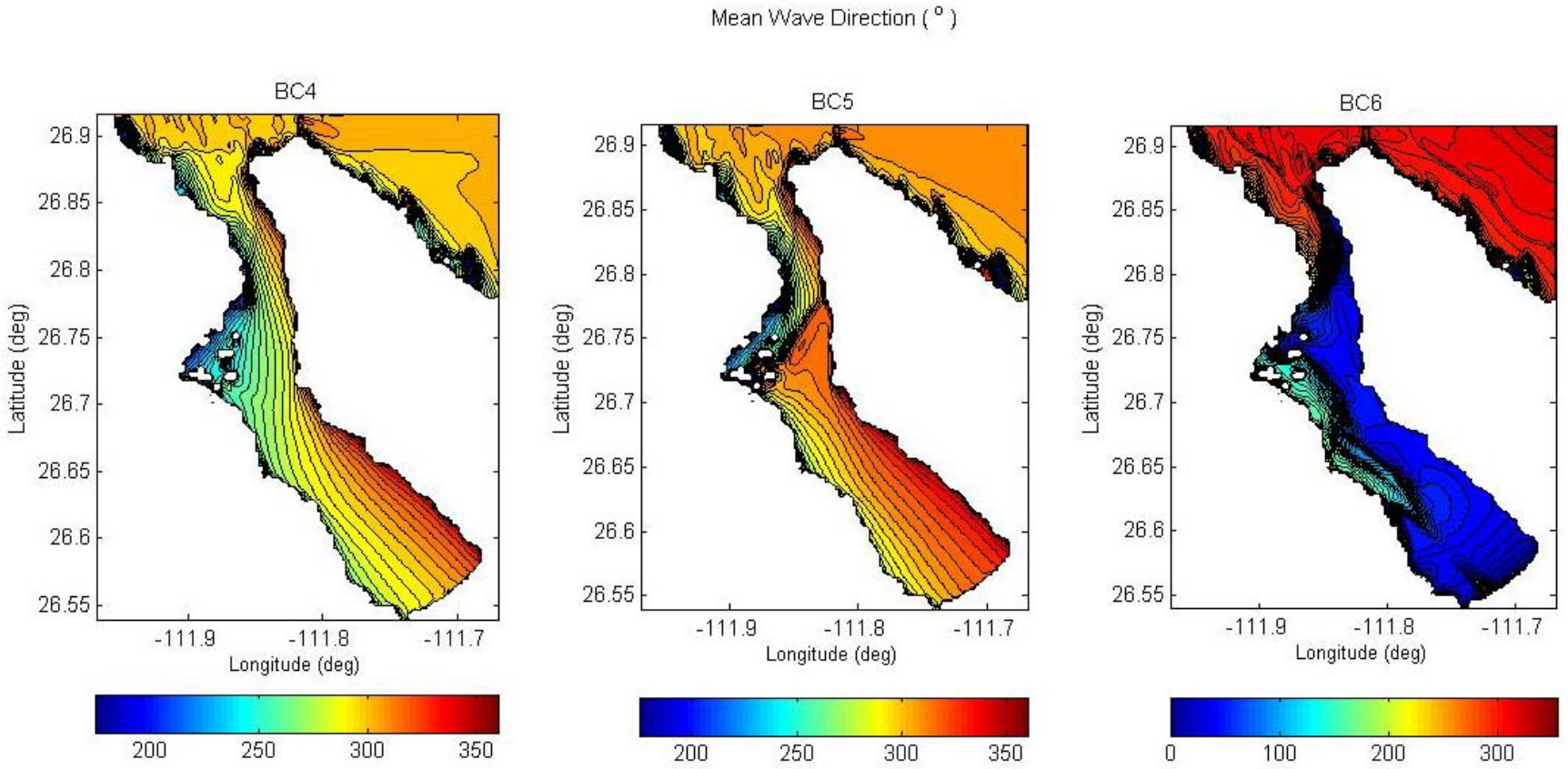

Figure 3-19 Mean Wave Direction Contours for BC4, BC5 and BC6

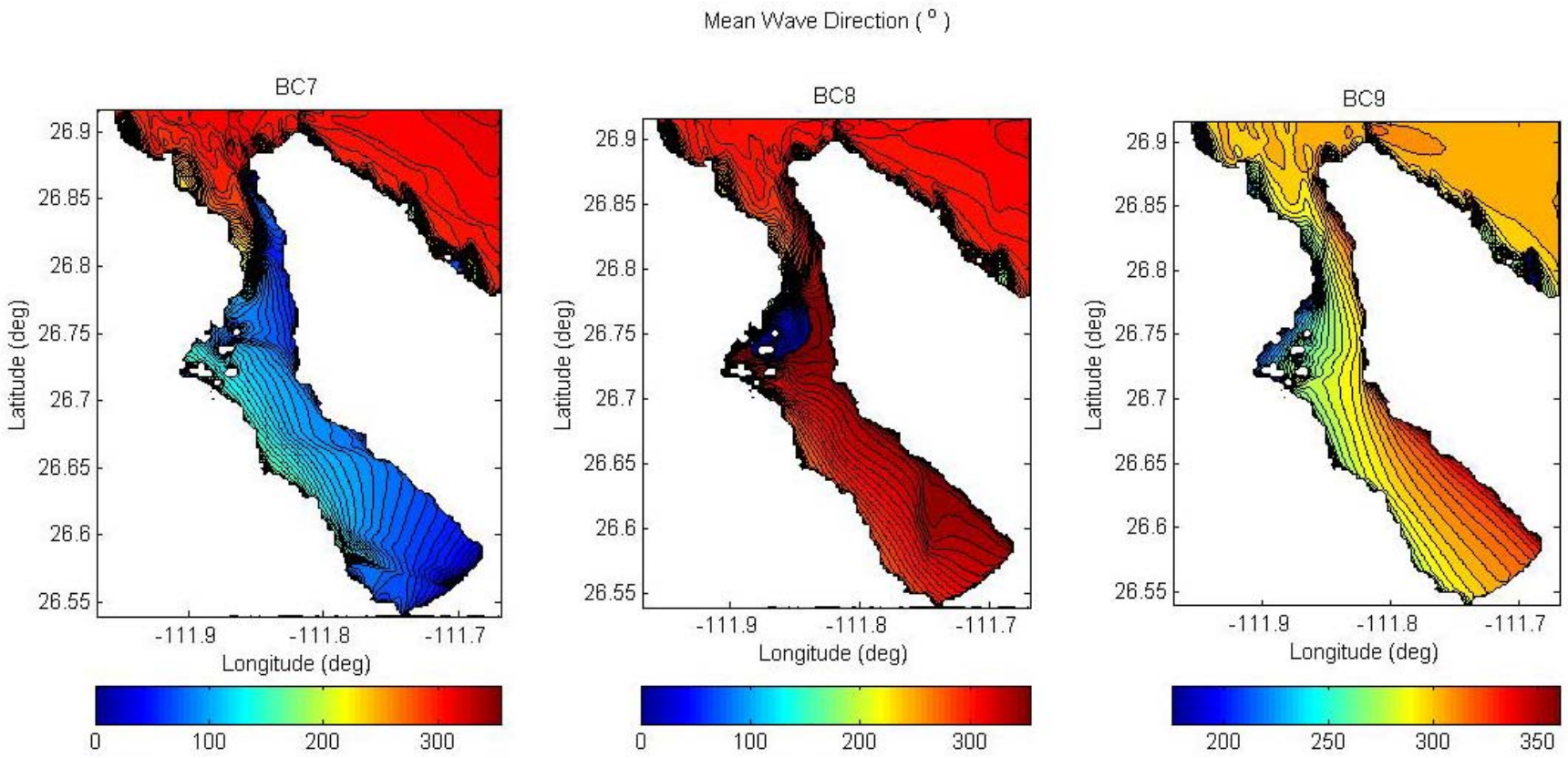

Figure 3-20 Mean Wave Direction Contours for BC6, BC7 and BC8

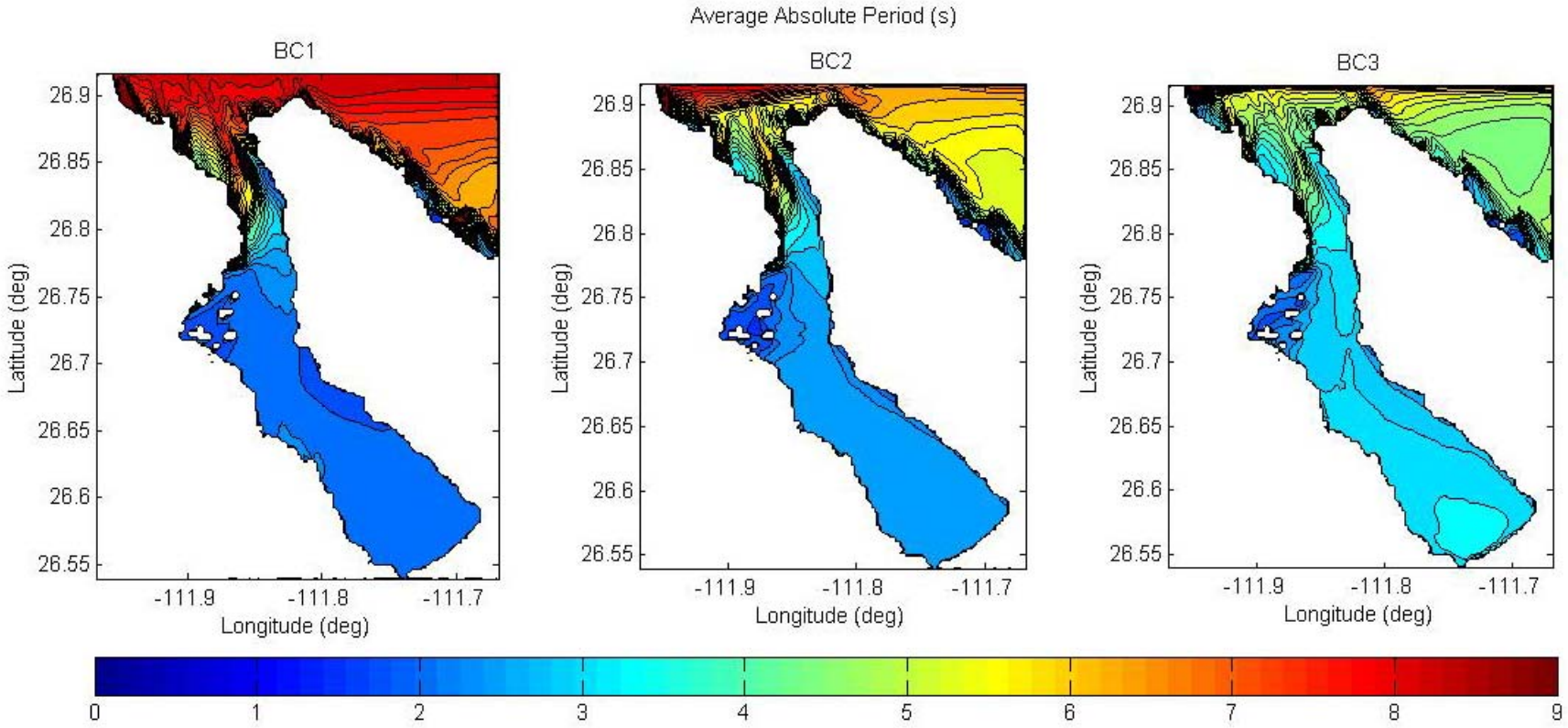

Figure 3-21 Average Absolute Period Contours for BC1, BC2 and BC3

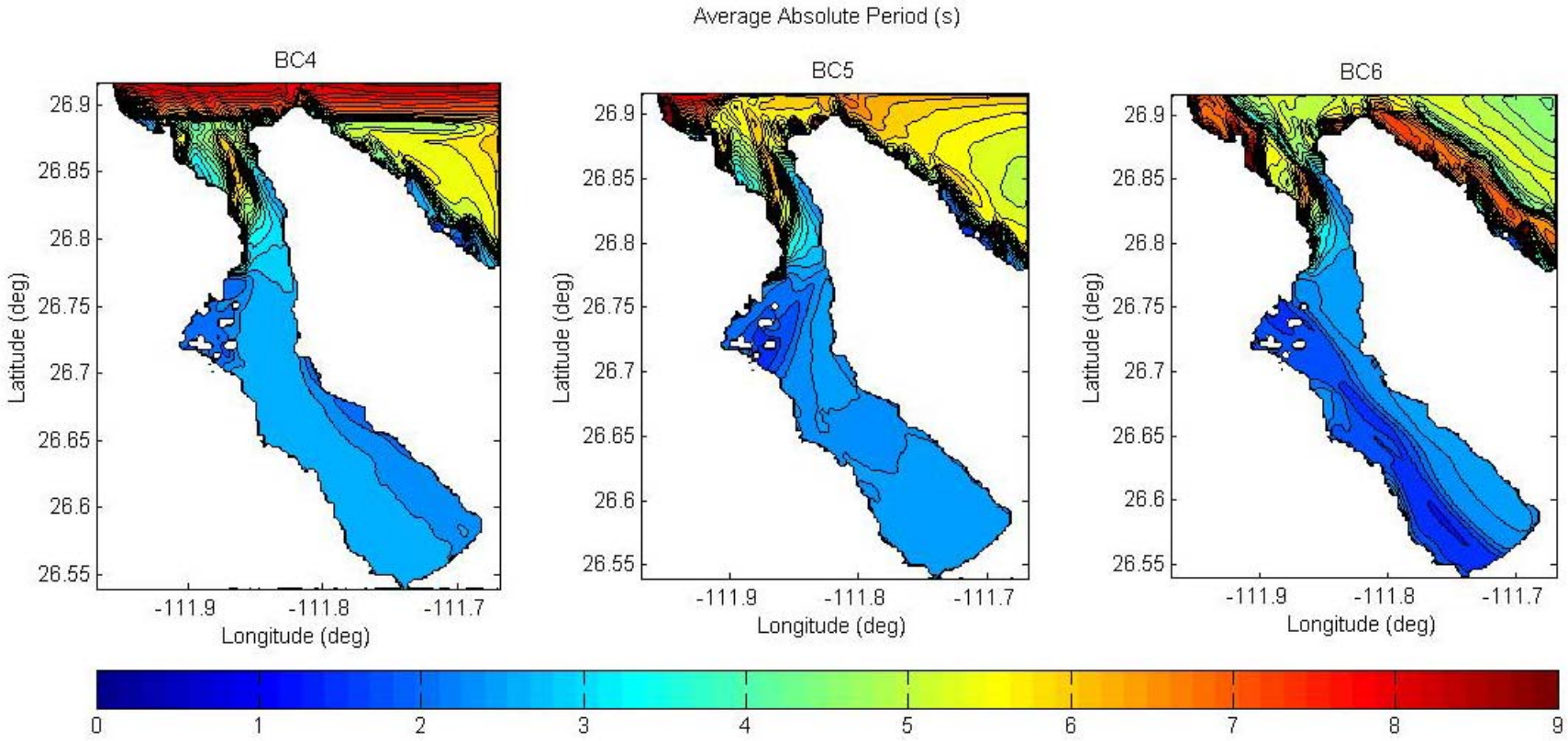

Figure 3-22 Average Absolute Period Contours for BC4, BC5 and BC6

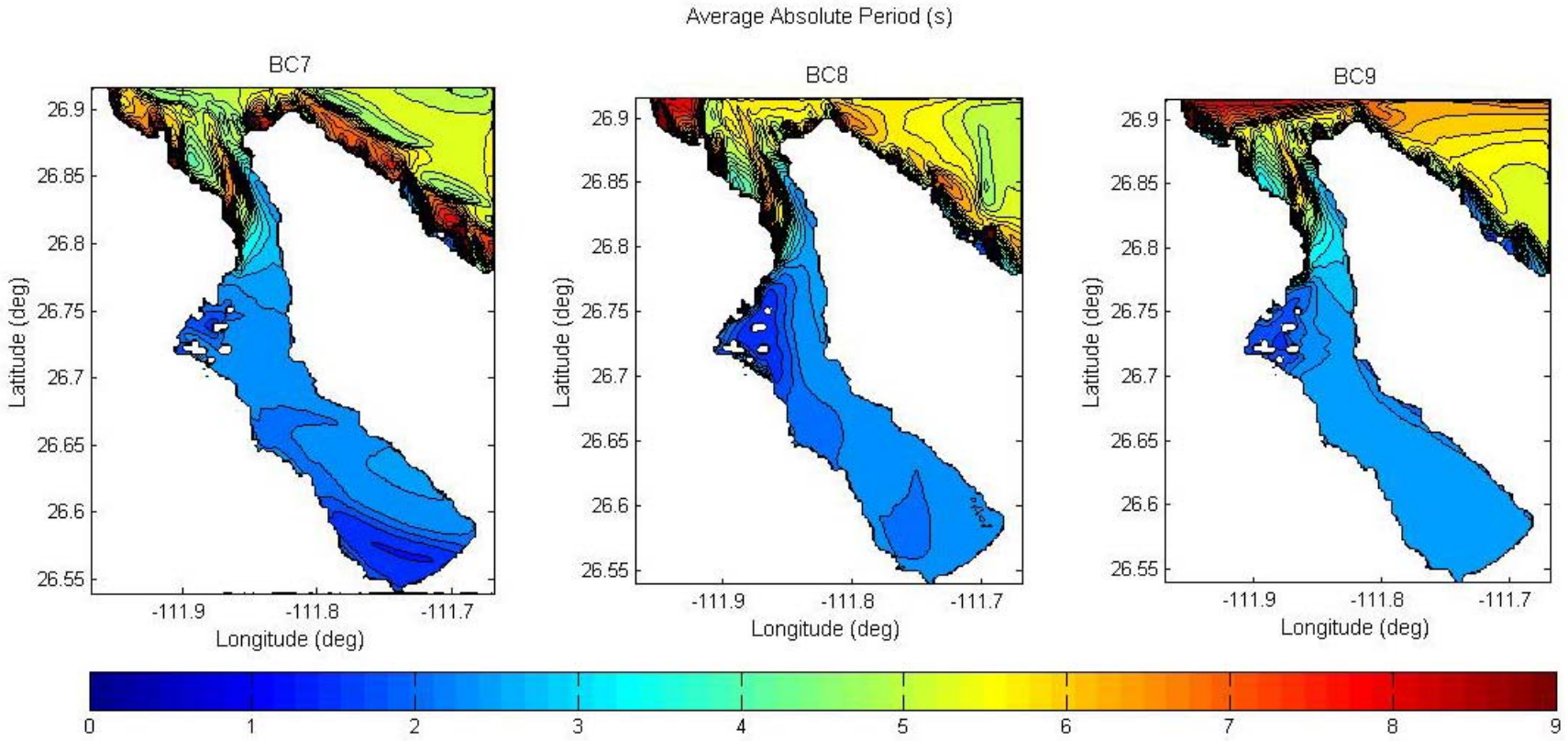

Figure 3-23 Average Absolute Period Contours for BC7, BC8 and BC9

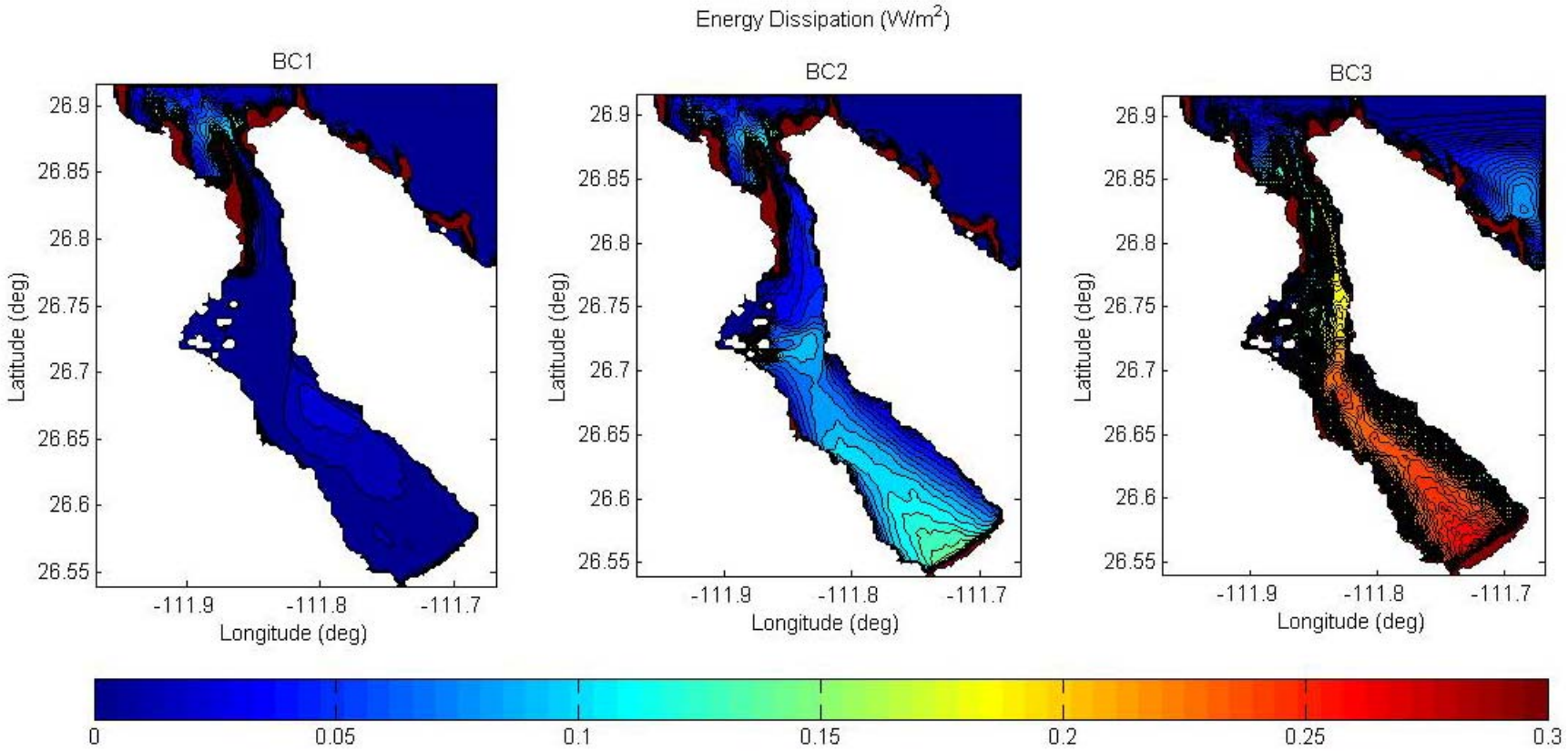

Figure 3-24 Energy Dissipation Contours for BC1, BC2 and BC3

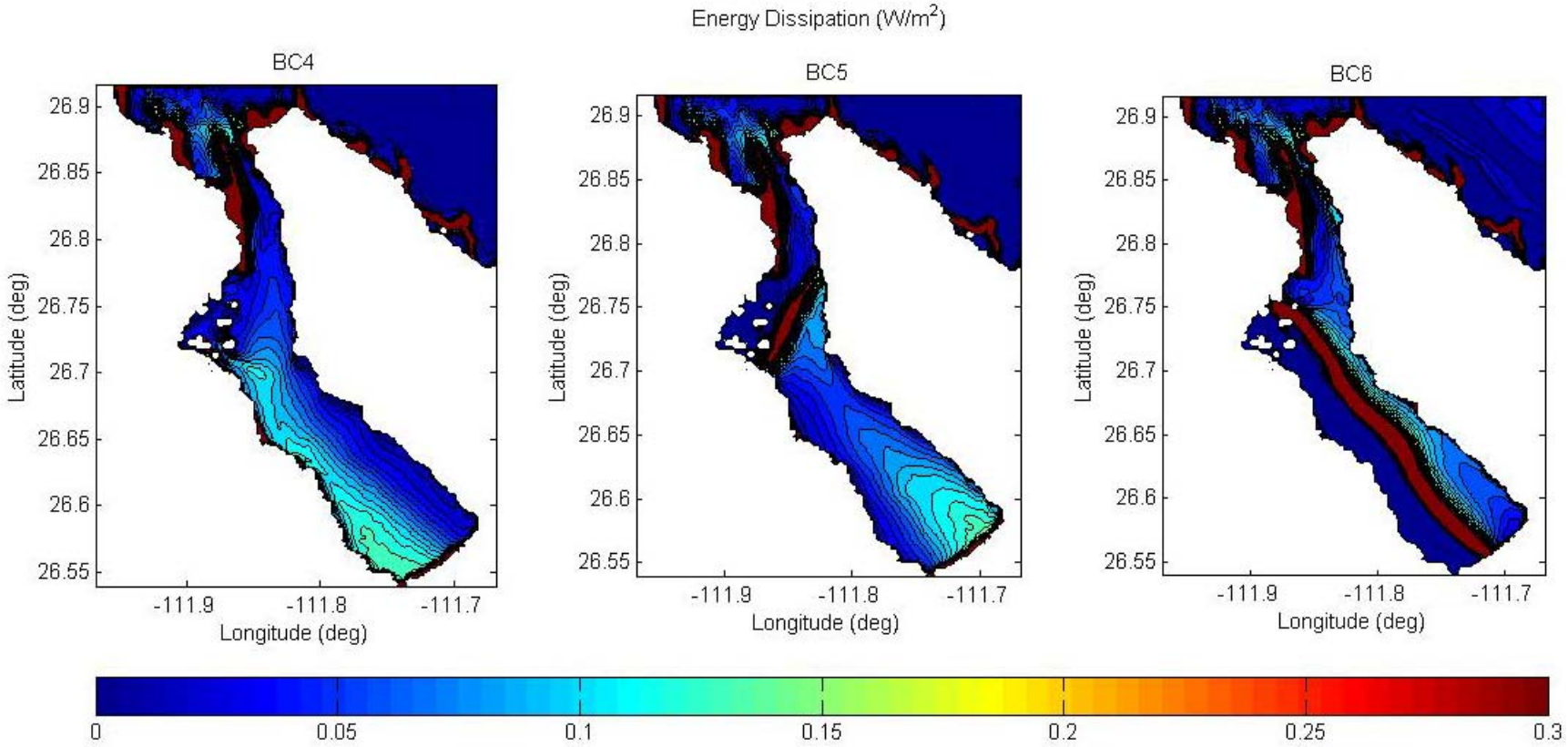

Figure 3-25 Energy Dissipation Contours for BC4, BC5 and BC6

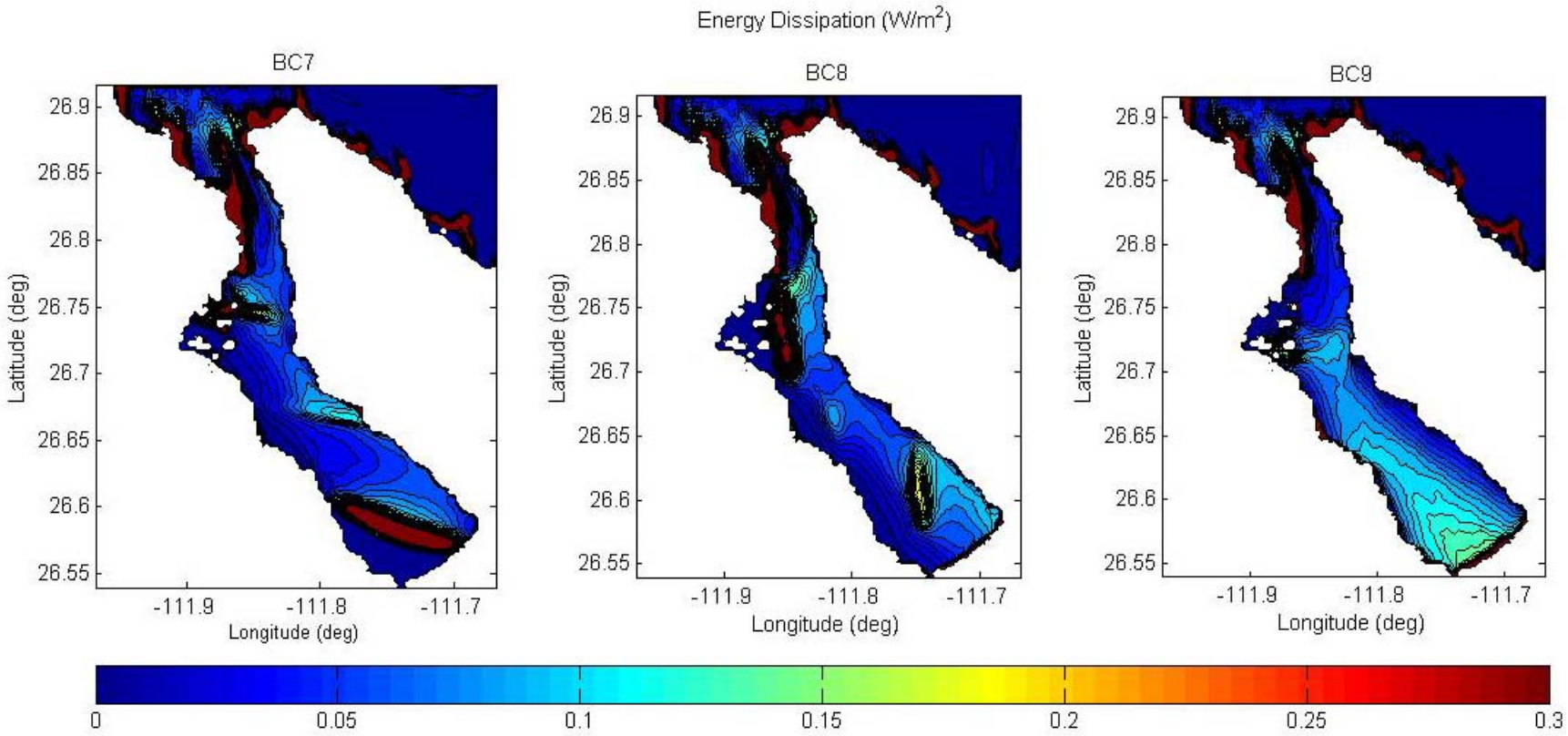

Figure 3-26 Energy Dissipation Contours for BC7, BC8 and BC9

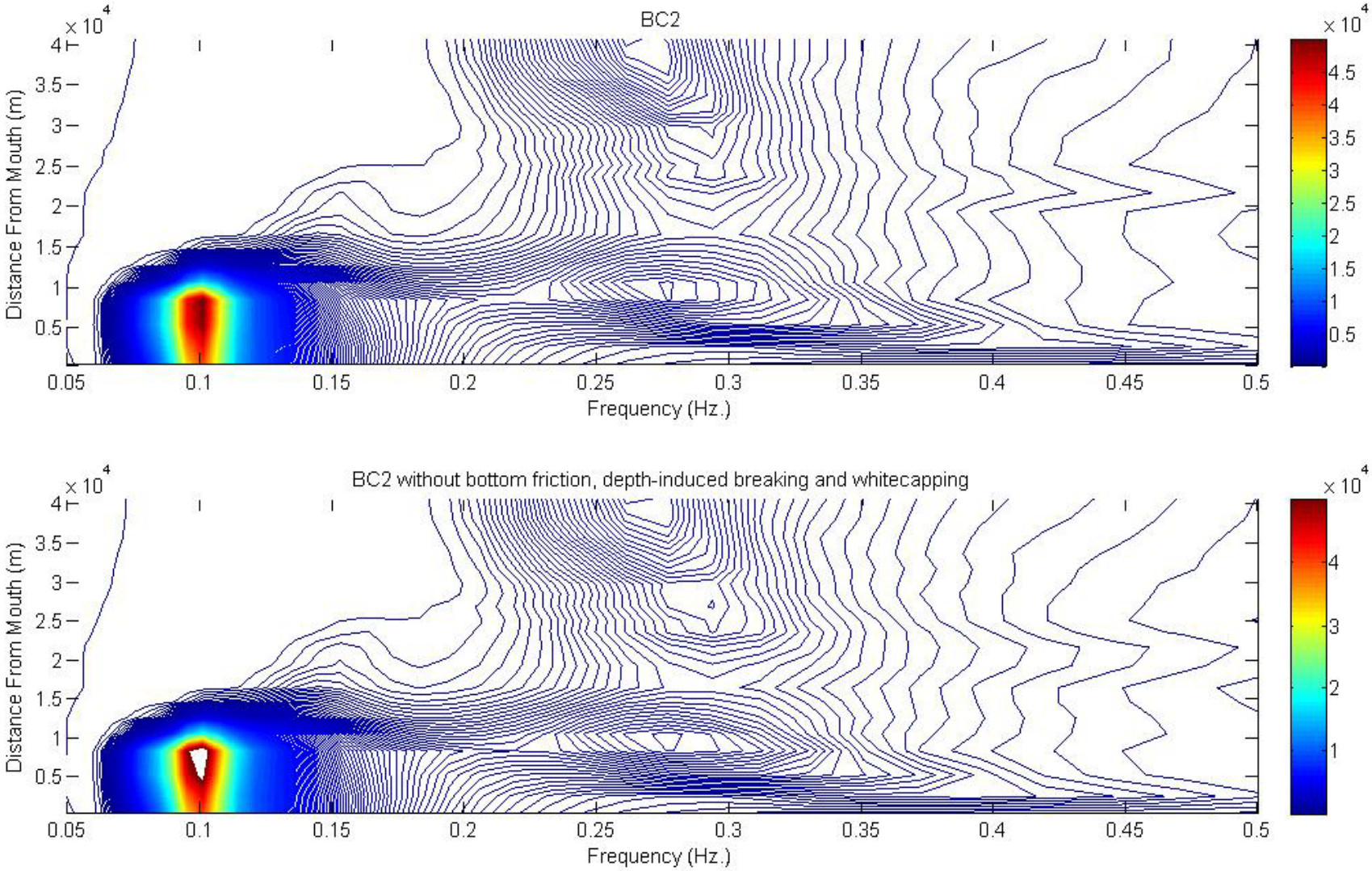

Figure 3-27 Spatial Energy Density Contours in J/m^2 for BC2 and the Case without Bottom Friction, Depth-Induced Breaking and Whitecapping

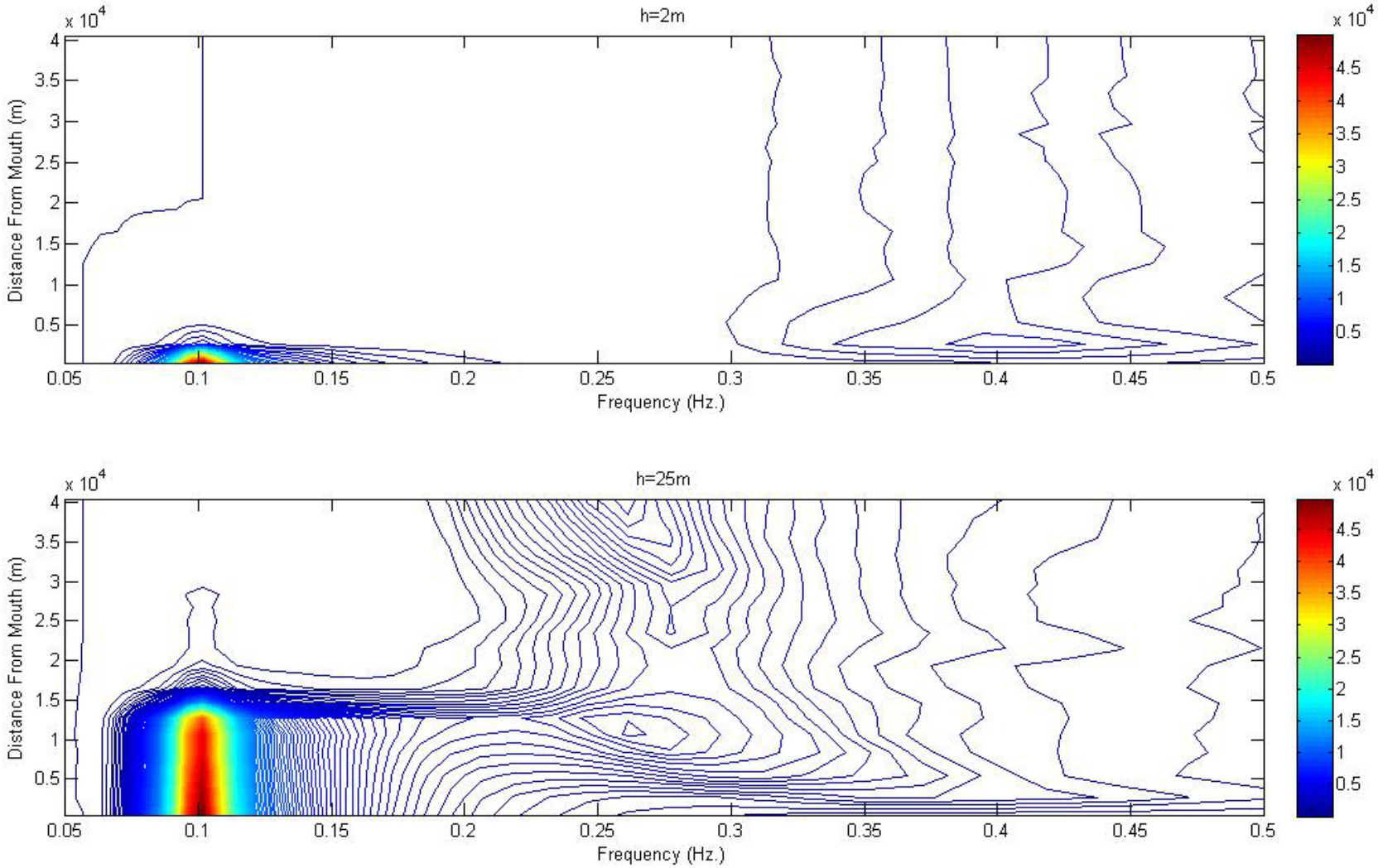

Figure 3-28 Spatial Energy Density Contours in J/m^2 for Flat Bottoms with Depths of 2 and 25 m

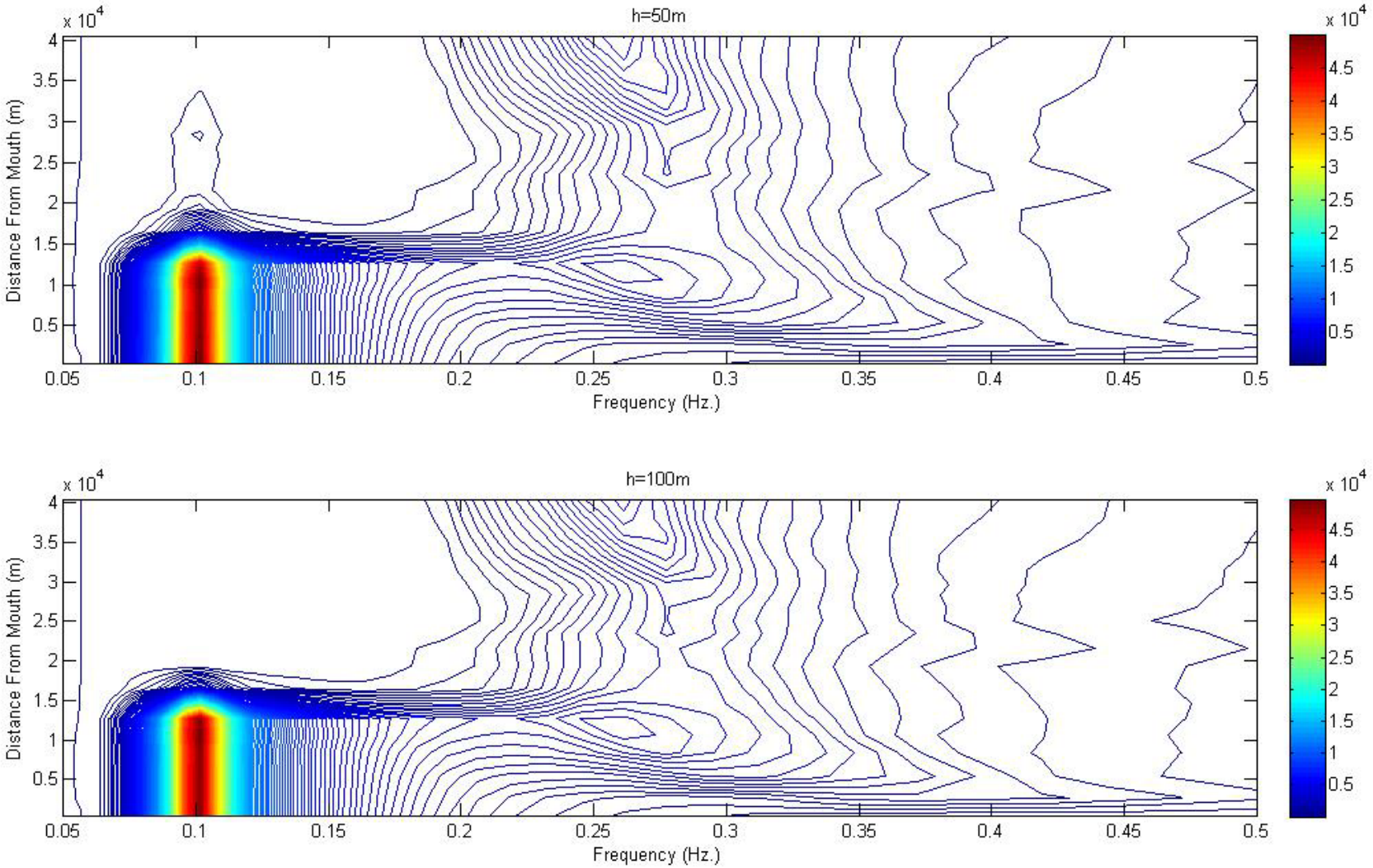

Figure 3-29 Spatial Energy Density Contours in J/m^2 for Flat Bottoms with Depths of 50 and 100 m

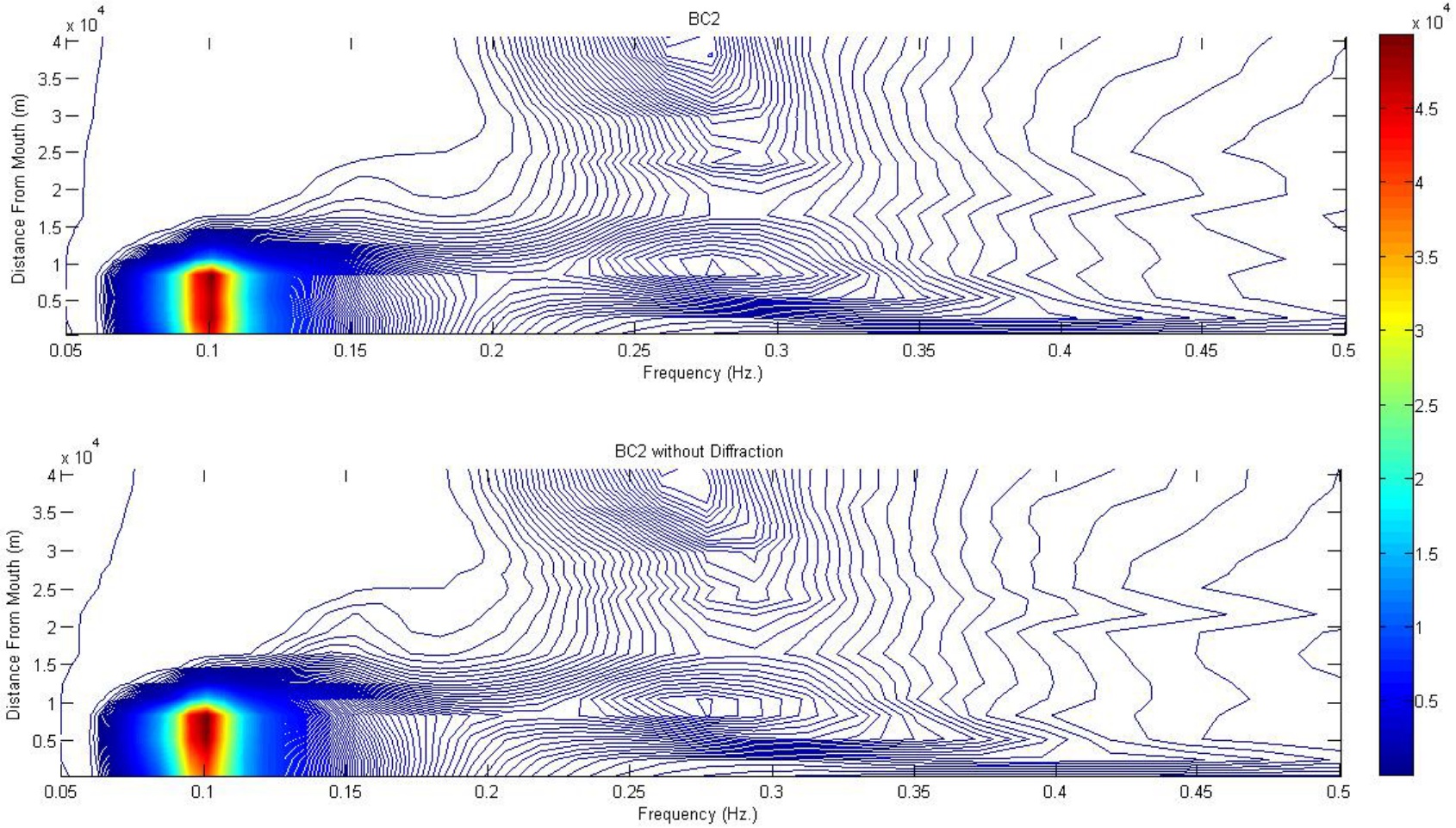

Figure 3-30 Spatial Energy Density Contours for BC2 and BC2 without Diffraction

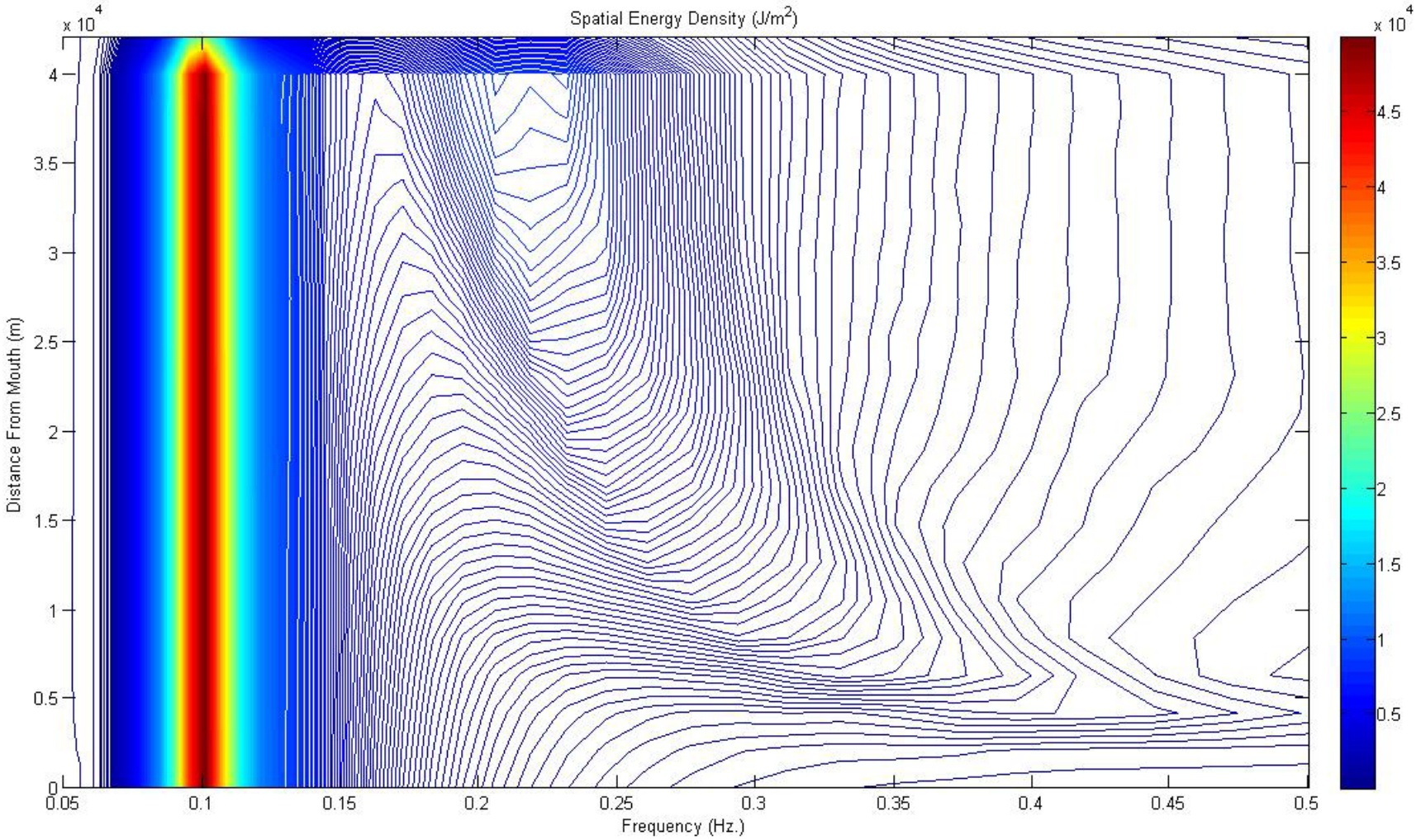

Figure 3-31 Spatial Energy Density Contours for a Flat Bottomed Rectangular Bay with a Depth of 100 m

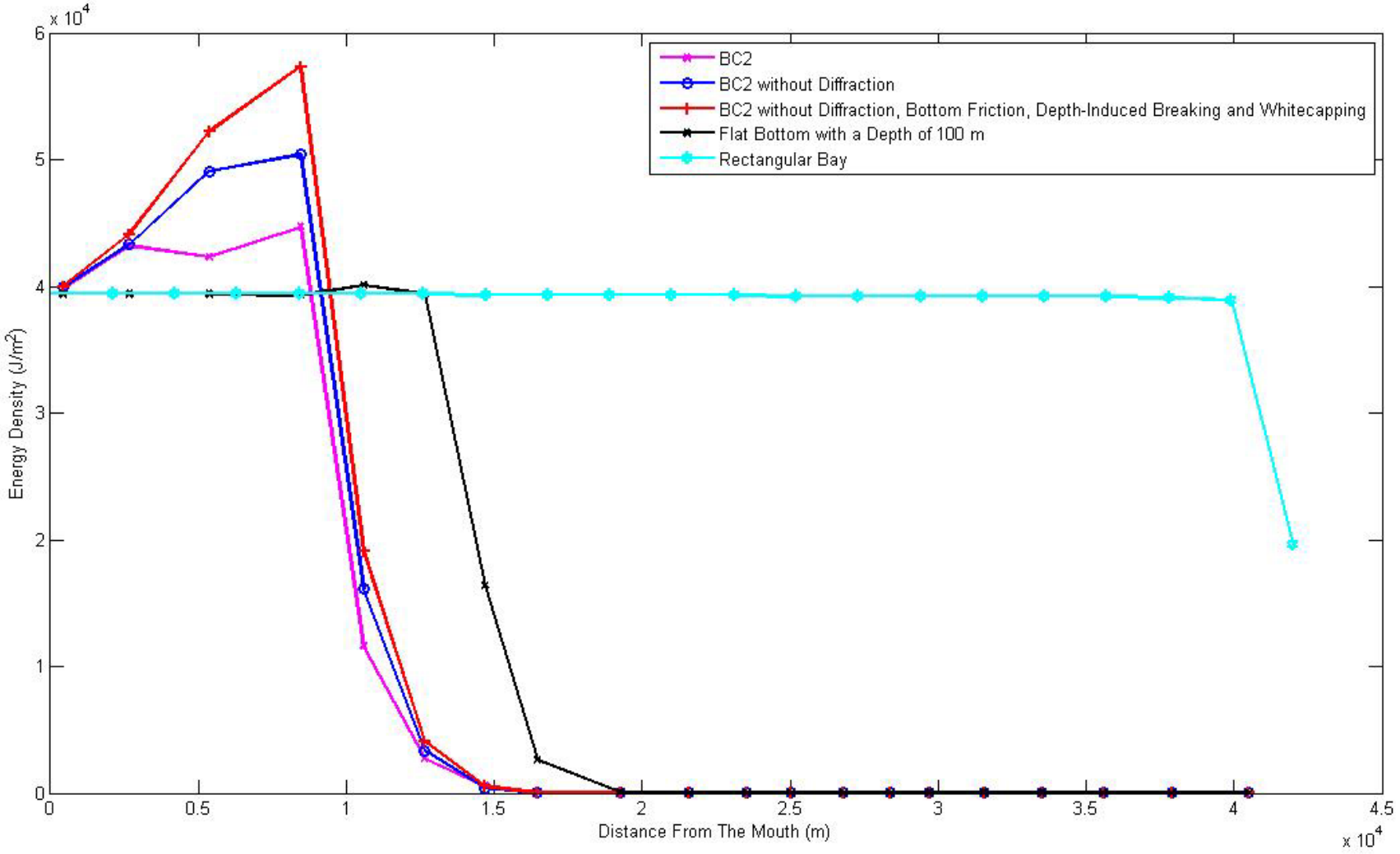

Figure 3-32 Distance from the Mouth vs. Energy Density Plots for Cases BC2; BC2 without Diffraction, BC2 without Diffraction, Bottom Friction, Depth-Induced Breaking and Whitecapping; Flat Bottom for Deep Water Conditions (Depth=100m) and Rectangular Bay without Diffraction, Bottom Friction, Depth-Induced Breaking and Whitecapping

CHAPTER 4
CONCLUSIONS

It has been observed both from the *in-situ* data and model results that the ocean swell waves were attenuated as they propagate into the bay and before reaching the head they completely disappeared. Moreover it was possible to observe locally generated high frequency wind waves all around the bay once again from both the observational and model results. Even though the data were not collected to study surface waves, results gathered from the model studies verified that the observational data have a revealing pattern of the surface waves.

The reasons behind the attenuation of the swell waves have found to be:

- Combined effect of bottom friction, depth-induced breaking and whitecapping,
- Diffraction,
- Refraction and,
- Wave blocking.

After observing the differences between the refraction eliminated case and the rectangular bay case, it has been seen that the geometry of the bay was reason for swell waves not to reach bay mouth. Waves were blocked by the land especially beyond 20 km into the bay. According to the calculations based on energy, 84% of the swell waves were blocked by the land before reaching the head. The contribution of refraction was 14%. Bottom friction, depth – induced wave breaking and whitecapping did not seem to have a significant effect on swell attenuation. The combined contribution of them was found to be around 1% to the attenuation. Diffraction's contribution was also found to be less than 1%.

LIST OF REFERENCES

Badan-Dangon, A., Dorman, C. D., Merrifield, M.A. and Winant, C.D. (1991). The lower atmosphere over the Gulf of California, *Journal of Geophysical Research* **96**, C9, pp. 16877-16896

Boon, J.D., Green, M.O., Suh, K.D. (1996). Bimodal wave spectra in lower Chesapeake Bay, sea bed energetics and sediment transport during winter storms, *Continental Shelf Research* **16**, pp. 1965-1988

Collins, J.I. (1972). Prediction of shallow water spectra, *Journal of Geophysical Research* **77**, 15, pp. 2693-2707

Dean, R. G., and Dalrymple, R. A. (1991). Water Wave Mechanics for Engineers and Scientists. 2nd ed., Prentice-Hall, Englewood Cliffs, NJ.

Hasselman, K., Barnett, T. P., Bouws, E., Carlson, H., Cartwright, D. E., Enke, K., Ewing, J. A., Gienapp, H., Hasselman, D. E., Kruseman, P., Meerburg, A., Müller, P., Olbers, D. J. , Richter, K., Sell, W. and Walden, H. (1973). Measurements of wind – wave growth and swell decay during the Joint North Sea Wave Project (JONSWAP), *Deutschen Hydrograhischen Zeitschrift*, 12, A8

Hasselmann, K., Allender, J. H., Barnett, T. P. (1985). Computations and parameterizations of the nonlinear energy transfer in a gravity wave spectrum. Part II: Parameterizations of the nonlinear energy transfer for application in wave models, *Journal of Physical Oceanography* **15**, pp. 1378-1391

Jeffreys, J. (1924). On the formation of the waves by wind, *Proceedings of the Royal Society of London*, A, pp. 107-189

Long, C.E., Oltman-Shay, J.M. (1991): Directional characteristics of waves in shallow water, *Technical Report CERC-91-1, U.S. Army Engineer Waterways Experiment Station*

Madsen, O. S., Poon, Y. K. and Graber, H. C. (1988). Spectral wave attenuation by bottom friction:Theory, *Proc. 21st Int. Conf. Coastal Engineering*, ASCE, pp. 492-504

Marione, S.G., Lavin, M.F. (2003). Residual flow and mixing in the large islands region of the Gulf of California, *Nonlinear Processes in Geophysical Fluid Dynamics*, Kluwer Academic, Dordrecht, The Nederlands, pp. 213-236

Mitsuyasu, H. (1997). On the contribution of swell to sea surface phenomena, *International Journal of Offshore and Polar Engineering* **4**, V7, pp. 241-245

BIOGRAPHICAL SKETCH

The author was born in Ankara, Turkey on January 16th 1984. She lived in her hometown Ankara for most of her life. She completed her primary, middle and high school education at Buyuk High School, Ankara between September 1990 and June 2001. Then she was accepted to the Civil Engineering program of Middle East Technical University, Ankara, in September 2001. During her undergraduate education she developed a special interest in Coastal Engineering after taking several courses on this area and she decided to seek a Master's degree on Coastal Engineering. After her graduation from collage in June 2005, she moved to Gainesville/Florida to obtain her Master's of Science degree in Coastal and Oceanographic Engineering from University of Florida.